Title:

Tumor-Draining Lymph Node–Derived CD8$^+$ T Cells Sustain Durable Systemic Immunity after Neoadjuvant IL-15 and PD-1 Blockade

Authors:

†Tatiana Delgado Cruz[1], †Rachel Honigsberg[1,2,4], Geoffrey J. Markowitz[1], Dicle Özge Özgenel[1], Arshdeep Singh[1], Meixian Stephanie Tang[1], Stella A Martomo[6], Liron Yoffe[3], Yongfeng He[1], Yang Bai[1], Jeegar Patel[7], Marissa M. Michael[1], Mitchell Martin[1], Timothy E. McGraw[5,1], Olivier Elemento[2], Nasser K Altorki[1], Vivek Mittal[1] & Jonathan Villena-Vargas[1*].

Afiliations:

1. Department of Cardiothoracic Surgery, Weill Cornell Medicine, New York, NY, USA
2. Englander Institute for Precision Medicine, Weill Cornell Medicine, New York, NY, USA
3. Department of Radiation Oncology, Weill Cornell Medicine, New York, NY, USA
4. Meinig School of Biomedical Engineering, Cornell University, Ithaca, NY, USA
5. Department of Biochemistry, Weill Cornell Medicine, New York, NY, USA
6. Evolve Immune Therapeutics, Branford, CT, USA
7. Evommune, New York,NY,USA.

† Co-first authors

Weill Cornell Medicine

525 East 68th Street

New York, New York 10065, USA

* Correspondence: jov9069@med.cornell.edu and tac4002@med.cornell.edu

Keywords: Lung cancer, immunotherapy, single-cell sequencing, T cells

Competing interests: All authors declare no potential conflicts.

One sentence summary:

Neoadjuvant IL-15 with PD-1 blockade expands lymph node clonal diversity and preserves stem-like $CD8^+$ T cell features, yielding superior antitumor efficacy, durable memory, and reduced metastatic recurrence.

Abstract:

The tumor-draining lymph node (tdLN) serves as a critical reservoir of tumor-reactive T cells, yet its contribution to preventing metastatic recurrence remains poorly understood. In this study, we investigate $CD8^+$ T cell clonal dynamics and memory responses induced by neoadjuvant anti–PD-1 therapy. We demonstrate that PD-1 blockade promotes the emergence of protective $CD8^+$ T cell memory, enriched with tumor-relevant clones that persist in the lymph nodes of long-term survivors. Furthermore, we show that combination of a neoadjuvant IL-15 superagonist with PD-1 blockade significantly increases clonal diversity, cytotoxicity, and clonal persistence in non-draining lymph nodes. These changes result in enhanced systemic antitumor immunity and durable memory that prevents tumor relapse. Our findings establish the tdLN as a critical immunologic hub that can be therapeutically targeted by IL-15 to augment PD-1 blockade efficacy and support a rationale for a phase II neoadjuvant combination immunotherapy trial in early-stage NSCLC.

49 **Main Text:**

50 **Introduction**

51 PD-1/PD-L1 immune checkpoint blockade (ICB) reinvigorates a population of exhausted $CD8^+$ T cells in
52 the primary tumor, but these cells possess limited functional capacity[1]. Moreover, clinical and
53 preclinical evidence indicates that PD-1 ICB relies heavily on a progenitor-like, $TCF1^+PD\text{-}1^+CD8^+$ T cell
54 subset[2]. Preclinical studies in cancer and chronic antigen models demonstrate that tumor draining lymph
55 nodes (tdLNs) harbor stem-like $CD8^+$ T cells ($TCF1^+$, $PD\text{-}1^+$), and acquire distinct transcriptional profiles
56 and functional states upon tumor infiltration[3, 4]. Furthermore, local PD-L1 blockade at the tdLN level
57 enhances tumor seeding by $CD8^+$ T cells in melanoma[5]. However, therapeutic strategies that
58 simultaneously reinvigorate pre-existing tumor-reactive T cells and generate new, functionally potent T
59 cell responses remain an area of active investigation.

60 Surgically resectable non-small cell lung cancer (NSCLC) is an aggressive disease in which most patients
61 receive multimodality therapy yet still face metastatic relapse rates of approximately 55%. Most patients
62 do not respond to anti-PD-1 therapy (aPD-1) alone or in combination with chemotherapy [6], prompting
63 strong interest in novel combination therapies to enhance T cell function through immunomodulation. [7].
64 Cytokines such as IL-2 are of significant interest as they act as T cell growth factors that provide strong
65 positive signals for anti-tumor activity [8]. IL-15 and IL-2 share common receptor subunits and overlap
66 in several biological functions, including proliferation of activated T cells, and promotion of cytolytic
67 effector $CD8^+$ T cell differentiation[9]. Unlike IL-2, IL-15 uniquely supports memory formation and
68 persistence of $CD8^+$ T cells[10] and promotes self-renewal of precursor exhausted $CD8^+$ T cell subsets
69 rather than rescuing terminally differentiated effectors[11]. We reasoned that generating a pool of long-
70 lived, tumor-specific memory T cells with IL-15 agonism could provide superior protection against post-

71 surgical metastatic relapse, which accounts for the majority disease-related mortality after definitive
72 resection.

73 In this work we define the role of lymph node–derived $CD8^+$ T cells as primary mediators of therapeutic
74 efficacy in resectable NSCLC. PD-1 ICB depends on tdLNs $CD8^+$ T cells for both primary antitumor
75 activity and the generation of functional memory. The addition of a neoadjuvant IL-15 superagonist
76 augments this response through a lymph node–directed "effector upgrade" that increases clonal diversity
77 of the $CD8^+$ T cell repertoire, enhances primary tumor clearance, sustains systemic T cell persistence, and
78 prevents late metastatic relapse at distant sites as well as systemic tumor rechallenge. This cell fate
79 programming originates in the tdLN, and the lymph node response is essential for optimal efficacy. These
80 findings provide a strong rationale for lymph node preservation during ICB in surgically resectable disease
81 and identify the tdLN as a critical therapeutic target for immunomodulation in this setting.

82 **RESULTS**

83 ***Critical role of tdLN in mediating responses to neoadjuvant PD-1 blockade as evident in a murine***
84 ***model of NSCLC with metastatic recurrence following curative-intent resection of primary tumor***

85 To assess the functional role of CD8+ T cells in primary tumor control and the prevention of metastatic
86 recurrence following surgery, we employed a murine model of metastatic NSCLC encompassing primary
87 tumor resection and subsequent metastatic relapse by using the highly metastatic 344SQ ($Kras^{G12D}$
88 $p53^{R172H\Delta G}$) cell line[12]. Primary tumors were established in the right flank of 129sv mice to allow for
89 resection through survival surgery, along with resection of their draining lymph nodes and/or non draining
90 lymph nodes (ndLNs) on the opposite flank/axilla (**Fig. 1a)**. Fluorescence-guided mapping identified
91 ipsilateral axillary and inguinal LNs as tdLNs [13], whereas contralateral and distant LNs in either the
92 opposite inguinal, axillary or in the mediastinum were designated as ndLNs. Flow cytometry of tdLNs

93 during primary tumor growth revealed a distinctive population of PD-1^{+}CD8^{+} T cells displaying an
94 effector/effector-memory (T E/EM; CD62L^{-}CD44^{+}) phenotype with increased interferon-γ and Ki67
95 expression relative to ndLNs (**Fig. 1b, supplementary Fig. 1a, b**). These findings support the notion of a
96 localized, tumor-driven immunological response within the tdLN compartment.

97 This model exhibited heterogeneous responses to neoadjuvant PD-1 blockade, similar to other animal
98 models of NSCLC [14, 15] and mirroring the variability observed in clinical settings[16]. Around a third
99 of treated mice demonstrated a measurable reduction in primary tumor burden below control levels as
100 assessed by bioluminescence imaging (BLI) prior to surgical resection (**Supplementary Fig. 1c**), where
101 aPD-1 responders had an increased accumulation of IL-7Rα^{+}, and Ly6c^{+} E/EM T cell
102 populations(**Supplementary Fig. 1d, e**). Markers associated with CD8 T^{+} cell subsets in the lymph node
103 critical for tumor remission after immunotherapy or surgical resection[17, 18] and TCM
104 compartmentalization into lymph nodes during homing [19]. This model enabled BLI monitoring of
105 primary tumor dynamics and metastatic dissemination following surgery (**Fig. 1c, d**). Necropsy confirmed
106 metastatic disease with lesions found in the lung, chest wall, liver, and spine (**Fig. 1e**), consistent with the
107 metastatic patterns observed in NSCLC patients[20], establishing this model as a clinically relevant
108 platform for studying tumor progression and therapeutic response.

109 To define the functional contribution of the lymph node and assess whether tdLN-derived T cell migration
110 was required for therapeutic efficacy, anti–PD-1–treated mice received the sphingosine-1-phosphate (S1P)
111 receptor antagonist FTY720, starting six days before the first anti–PD-1 dose and continuing until primary
112 tumor resection to restrict T cell egress from tdLNs (**Fig. 1f**). Inhibition of T cell trafficking fully
113 abrogated the therapeutic benefit of neoadjuvant PD-1 blockade (**Fig. 1g**). These mice exhibited markedly
114 reduced infiltration of PD-1^{lo}CD8^{+} T cells in the tumor (**Fig. 1h**), while there was a higher proportion of
115 PD-1^{+} E/EM CD8^{+} T cells within the tdLNs, suggesting that FTY720 inhibited the migration of this

116 subpopulation to the tumor. These findings demonstrate that the efficacy of neoadjuvant PD-1 blockade
117 is critically dependent on tdLN-derived $CD8^+$ T cell migration to the primary tumor site.

118 We next investigated whether $CD8^+$ T cells were required for long-term immunological memory and
119 protection against metastatic recurrence. While all untreated mice developed metastatic disease by day 60
120 post-resection, approximately 15–20% of those treated with neoadjuvant anti–PD-1 remained metastasis-
121 free beyond this time point in multiple independent experiments (**Fig. 1i**). To determine whether $CD8^+$ T
122 cells were necessary for durable immunity, long-term responder mice **(Fig. 1j)** were depleted of $CD8^+$ T
123 cells prior to intravenous rechallenge with 344SQ tumor cells via tail vein injection (**Fig. 1k**). Peripheral
124 blood analysis confirmed efficient $CD8^+$ T cell depletion (**Supplementary Fig. 1f**). Critically, $CD8^+$ T
125 cell depletion abrogated tumor rejection upon systemic rechallenge showing similar tumor growth than
126 naïve age-matched controls. In contrast, non-depleted mice, eradicated tumor cells within a week with
127 100% of survival after rechallenge (**Fig. 1l, m**), establishing the requirement for memory $CD8^+$ T cells in
128 maintaining immune surveillance and controlling metastatic outgrowth.

129 Together, these findings demonstrate that the therapeutic efficacy of neoadjuvant PD-1 blockade in this
130 model is critically dependent on LN-derived $CD8^+$ T cells. Migration of these cells to the primary tumor
131 is required for primary tumor response, while $CD8^+$ T cell memory is essential for long-term immunity
132 and protection against metastatic relapse.

133

134 ***Neoadjuvant anti-PD-1 with IL-15 receptor alpha agonist enhances anti-tumor efficacy***

135 Augmentation of progenitor-like, $TCF1^+PD\text{-}1^+CD8^+$ T cells has been shown to be critical for efficacy of
136 PD-1 blockade. Combination therapies to achieve durable responses have shown promising results,
137 specially, the use of cytokines that provide positive signals for T cells[21]. IL-15 is integral for T cell

138 survival[22], furthermore it has also been shown that it can promote self-renewal of precursor-exhausted
139 $CD8^+$ T cells[11]. We hypothesized that combining neoadjuvant PD-1 blockade with an IL-15 agonist
140 would potentiate antitumor immunity by reprogramming $CD8^+$ T cells in the tdLN. To test this hypothesis,
141 we utilized an IL-15 superagonist KD033, a fusion immunocytokine that comprises a high-affinity anti–
142 PD-L1 antibody linked to the IL-15/IL-15Rα sushi domain complex. This design facilitates IL-15 trans-
143 presentation from PD-L1 expressing immune cells, increasing cytokine half-life and bioavailability while
144 minimizing antibody-dependent cellular cytotoxicity (ADCC)[23]. KD033 characterization showed that
145 antitumor efficacy in a colon carcinoma mouse model relied on $CD8^+$ T cells with a unique phenotype
146 characterized by upregulation of genes associated with cytotoxicity in contrast with untreated controls. It
147 was also shown that IL-15 component of KD033 was responsible for most of this phenotype, as changes
148 in gene signatures by this superagonist were recapitulated in a non-targeting variant (nt-KD033) only
149 comprising the IL15/15Rα fraction.

150 Neoadjuvant administration of a single IL-15Rα agonist dose, either alone or in combination with three
151 doses of anti–PD-1, significantly reduced primary tumor burden relative to anti–PD-1 monotherapy or
152 isotype control. By days 7–10 post-treatment, >90% of mice receiving combination therapy exhibited
153 reduced BLI signaling below control levels, compared with 30-50% under PD-1 blockade alone and 80%
154 with IL-15Rα agonist monotherapy (**Fig. 2a, b**). Longitudinal imaging over 200 days revealed that, IL-
155 15Rα in combination with PD-1 blockade substantially diminished metastatic recurrence (**Fig. 2c**) and
156 improved overall survival, with the majority of mice remaining alive at day 200 and in contrast with single
157 IL-15Rα or aPD-1 single treated groups were only 14% and 18% of the mice survived respectively (**Fig.
158 2d).**

159

160 ***Neoadjuvant IL-15 superagonist with anti-PD-1 drives cytotoxic, polyclonal CD8 T-cell responses from***
161 ***an effector/effector-memory precursor subset.***

162 To study how IL-15 agonism combined with aPD-1 results in higher antitumor efficacy and lower
163 metastatic recurrence compared to aPD-1 monotherapy, we first assessed $CD8^+$ T cell populations across
164 compartments at time of surgery using flow cytometry. Within the tdLN IL-15Rα, in combination with
165 PD-1 blockade, increased the proportion of $CD8^+$ T cells from total $CD3^+$ T cells from approximately 20%
166 to 50%, and proportionally expanded a population of effector/effector-memory IL-7$R\alpha^+$ T cells exhibiting
167 cytotoxic features, evidenced by increased IFN-γ expression (22% vs. 7%) when compared to PD-1
168 blockade alone. Similar changes were observed in the tumor, where $CD8^+$ T cells were more
169 proportionally expanded and exhibited increased granzyme B expression (90% vs. 40%), reduced PD-1
170 levels, and increased IL-7R expression (**Fig. 3a, b, supplementary Fig. 2a-d**).

171 To further understand $CD8^+$ T cell tumor specific responses induced by treatment, we performed paired
172 single-cell T cell receptor (TCR) and RNA sequencing following prior published methods[24, 25]. We
173 sorted $CD45^+CD3^+CD8^+$ T cells from tdLNs and tumors from mice treated with IgG, anti–PD-1, IL-15Rα
174 agonist, or combination therapy at the time of surgery (**Fig. 3c**). By leveraging TCR CDR3 sequences we
175 could identify tumor relevant expanded clones (n>2) present in the tdLN by TCR match or tumor matched
176 clones (TM), and study differences in CD8+ T cell clonal dynamics induced by treatment. TM clones
177 constituted approximately 23% of all $CD8^+$ T cells (total n = 20,223 TM clones), indicating a substantial
178 degree of clonal overlap between the tumor-and tdLN repertoires **(supplementary Fig. 3a)**.

179 Unsupervised UMAP clustering of expanded TM clones resolved eight transcriptionally distinct subsets
180 spanning memory-like to exhausted-like states (**Fig. 3d**). Memory-enriched clusters were characterized
181 by high expression of trafficking and homeostatic genes (*Sell, Ccr7, Klf2, Tcf7*)[25] and minimal

182 expression of cytotoxic or inhibitory receptor genes. In contrast, activated and exhausted-like subsets
183 upregulated cytolytic mediators (*Gzmb, Gzmf, Prf1, Ifitm 1, Ifitm 2, Ifitm 3, Nkg7, Klrk1*)[26] and
184 inhibitory receptors (*Tox, Havcr2, Pdcd1, Entpd1, Lag3, Ctla4*)[27]. These transcriptional patterns were
185 consistent with established T cell differentiation signatures.

186 TM clones exhibited marked tissue-dependent transcriptional clustering. Within the tdLN, 72% resided
187 within a single memory-like cluster, whereas in the tumor, clones were more widely distributed, with 47%
188 localized within activated clusters (clusters 0, 2, 4, 6, 7) (**Fig. 3e**). Differential expression analysis revealed
189 that tdLN TM T cells preferentially expressed genes linked to early differentiation and memory formation
190 (*Tcf7, Klf2, Il7r, Ly6c2*)[28], whereas tumor-infiltrating T cells upregulated transcripts associated with
191 activation, cytotoxicity, and inhibitory receptor engagement (*Gzmb, Prf1, Ifng, Havcr2, Pdcd1, Ctla4*),
192 (**Fig. 3f**)[29]. Modular scoring confirmed these transcriptional differences, with tdLN TM clones
193 displaying a naïve/central memory-like signature, while their tumor-infiltrating counterparts exhibited
194 increased effector and terminal exhaustion scores (**Supplementary Fig. 3b, c**). Consistent with these
195 observations, tdLN TM clones expressed *Tcf7* and *Il7r*, markers of long-lived memory, while tumor-
196 infiltrating clones displayed high *Pdcd1* and *Havcr2* expression, indicative of progressive differentiation
197 and exhaustion.

198 Examining $CD8^+$ T cell distribution following neoadjuvant therapy revealed significant treatment-
199 dependent shifts. Within the primary tumor, IL-15Rα agonist treatment, alone or in combination with PD-
200 1 blockade, enriched clones within a cytotoxic cluster (cluster 0) characterized by elevated expression
201 of *Gzma, Id2,* and *Eomes*, whereas PD-1 blockade or IgG alone predominantly localized clones to cluster
202 2, which exhibited high inhibitory receptor expression (*Tigit, Tox, Lag3, Pdcd1*)[30]. Within the tdLN, all
203 treatment regimens showed most TM clones primarily within the memory-like cluster 1 while also
204 increasing representation in clusters 3 and 5, which were enriched for chemotaxis- and proliferation-

205 associated gene programs **(Fig. 3g, h)**. Notably, IL-15Rα agonism and PD-1 blockade induced distinct
206 transcriptional programs in the tdLN, suggesting divergent mechanisms of immune modulation. PD-1
207 blockade preferentially upregulated AP-1 family transcription factors and memory-associated genes such
208 as *Lef1, Ccr7,* and *Sell*. In contrast, IL-15Rα agonist therapy drove a transcriptional profile marked by
209 heightened cytotoxicity, activation, and migratory potential, with increased expression of KLR-associated
210 transcripts (*Klrk1, Ifitm 1, Ifitm 2, Ifitm 3*)[31] within both the tdLN and tumor and *Gzmb* in clones within
211 the tumor **(Fig. 3i).**

212 Collectively, these findings demonstrate that neoadjuvant therapy profoundly shapes the differentiation
213 trajectory of TM $CD8^+$ T cells across tissue compartments. IL-15Rα agonist therapy, alone or in
214 combination with PD-1 blockade, drives a highly cytotoxic and activated phenotype, whereas PD-1
215 blockade alone preferentially enriches for clones with high inhibitory receptor expression. Furthermore,
216 clones within the tdLN retain a progenitor-like, memory-like associated state, serving as a reservoir for
217 differentiated, cytotoxic effectors within the tumor—a process that is further potentiated by IL-15Rα
218 agonism.

219

220 ***Treatment related CD8+ T cell clone diversity and cell fate originates in the tdLN***

221 To determine how neoadjuvant interventions influence $CD8^+$ T cell clonal diversity, we assessed the
222 impact of treatment on unique expanded TM clones. Mice receiving anti–PD-1 or IL-15Rα agonist therapy
223 exhibited increased TM clonal diversity relative to isotype controls (14 clones), averaging 22 and 45 TM
224 clones, respectively, while combination therapy yielded 43 TM clones **(Fig. 4a)**. These findings indicate
225 that while both PD-1 blockade and IL-15Rα broaden the CD8+ T cell repertoire, IL-15Rα notably
226 enhances clonal diversity. Further analysis revealed that memory-enriched cluster 1 exhibited the greatest

227 increase in clonal diversity, with 90% of tdLN-localized TM clones residing within this subset. IL-15Rα-
228 treated and combination-treated mice exhibited 28 and 24 unique clones, respectively, compared to only
229 3 and 5 in IgG and aPD-1 treated mice **(Fig. 4b, c)**. These data suggest that IL-15Rα expands clonal
230 diversity primarily within a progenitor-like subset in the lymph node with stem-like features.

231 To further dissect the heterogeneity within the memory cluster, we identified its constituent subclusters.
232 Differential expression analyses revealed that tdLN clones within this memory state exhibited a
233 progenitor-like phenotype (*Klf2, Il7r, Tcf7*), whereas tumor-infiltrating clones expressed genes associated
234 with cytotoxicity and activation (*Gzmb, Pdcd1, Ifngr1*) (**Fig. 4d**). Memory T cells were further subdivided
235 into five transcriptional subclusters (MC) based on the highest relative genes expressed: early cytotoxic
236 effector/ effector memory-like (MC0), Il7r-high (MC1), glycolysis-associated (MC2), naïve/central
237 memory/progenitor-like (MC3), and Klf2-high trafficking/activation memory-like (MC4) (**Fig. 4e**).Most
238 tdLN T cells were concentrated in early differentiation states (MC1, MC3, MC4), while T cell clones in
239 tumor concentrated in clusters MC0, MC2, MC5 and MC4 (**Fig. 4f**). Differential expression analysis
240 between PD-1 and combination therapy within tdLN T cells revealed that PD-1 blockade upregulated
241 progenitor/exhausted-like genes (*Sell, Tcf7, Tox, Slamf6*), whereas combination therapy enriched for
242 cytolytic markers (*Ifitm1, Ifitm2, Ifitm3, Gzma, Klrk1*) (**Fig. 4g**), with IL-15Rα treatment preferentially
243 increasing the proportion of MC1 T cell clones (**Fig. 4h, i**) and significantly increasing the KILRK-1/IL-
244 7Ra (KILR Effector) modular score. By contrast, PD-1-treated and IgG-treated memory T cells remained
245 predominantly in MC3 and exhibited a progenitor-like transcriptional signature [32](**Fig. 4j**).

246 These transcriptional differences extended to tumor-infiltrating T cells, where IL-15Rα therapy increased
247 the representation of MC0 and significantly elevated the KILR Effector score relative to non-IL-15Rα-
248 treated mice. Notably, PD-1 blockade or IgG treatment failed to enhance KILR effector function from
249 tdLN to tumor, whereas IL-15Rα treatment facilitated this transition, aligning with the findings of our

250 flow cytometry data **(Fig. 3b, c).** This data suggest that IL-15Rα agonism drives an effector memory
251 phenotype with cytotoxic features that initiates in the tdLN ultimately shaping tumor effector function
252 upon tumor infiltration.

253

254 ***CD8 T-cell clonal persistence is enhanced by IL-15Rα agonist***

255 Having established that IL-15Rα agonist therapy significantly prolongs median survival compared to IgG
256 or PD-1 blockade alone, we next investigated the systemic persistence and phenotype of $CD8^+$ T cell
257 across lymphoid compartments by phenotyping ndLNs (contralateral inguinal) of recurrence-free mice
258 between 30 and up to 120 days post-treatment **(Fig. 5a)**. These surviving, tumor-free mice demonstrated
259 a higher proportion of central memory-like (TCM; $CD62L^+CD44^+$) $CD8^+$ T cells within ndLNs. IL-15Rα
260 agonist in combination with PD-1 blockade significantly increased the percentage of $CD8^+$ T cells (37%
261 vs. 25%) and TCM subsets (20% vs. 14%) compared to PD-1 blockade alone. Additionally, combination
262 therapy markedly enhanced the proportion of IL-7Rα expressing T cells within the TCM subset, which
263 uniformly expressed high levels of TCF-1 (**Fig. 5b, supplementary Fig. 4a-d**).

264 Given the distinct clonotypic and differentiation profiles across treatments we observed at time of tumor
265 resection and to evaluate persistence of tumor specific clones more than 30 days after surgery, we
266 conducted scTCR and RNA sequencing in ndLNs (mediastinal or contralateral inguinal) from mice
267 previously sequenced, thus using initially identified TCRs to tumor-match clones in the ndLN. UMAP
268 analyses encompassing clones from initial tumor, tdLN and 30+ days ndLN, revealed close proximity
269 between ndLN and tdLN clones **(Fig. 5c),** an observation consistently evident at the level of individual
270 persistent clones (**Supplementary Fig. 5a-c**). While tumor clones exhibited decreased expression of
271 memory-associated genes, including *Tcf7*, *Il7r*, and *Ly6c2* , TM clones in the tdLN and ndLNs showed

272 higher expression of these markers**.** Clonal-average score showed tumor-infiltrating clones had relative
273 reduced quiescence and memory signature and increased cytotoxic effector markers compared to ndLN
274 and tdLN counterparts **(Fig. 5d)**.

275 Clonotypic tracking by treatment groups demonstrated that neoadjuvant therapy markedly enhanced the
276 persistence of tumor-matched clones in ndLNs beyond day 30, with IL-15Rα agonist alone or in
277 combination with PD-1 blockade doubling the proportion of persistent clones compared to PD-1 blockade
278 monotherapy and in contrast to IgG control where almost no persistent clones were found (**Fig. 5e**).
279 Importantly, persistent clones in IL-15Rα and combination therapy groups displayed heightened
280 expression of IL7Rα compared to PD-1 blockade alone as well as showed an enhanced KILRK1/IL-7R
281 (KILR effector) signature within tdLN T cells at the time of resection. (**Supplementary Fig. 5d, e**).

282

283 ***IL-15Rα agonism depends on the tdLN for establishment of primary antitumor response and memory,***
284 ***which relies on both CD8$^+$ and CD4$^+$ T cells***

285 To evaluate the role of the tdLN in primary antitumor efficacy and systemic memory in IL-15Rα+aPD-1
286 treated mice, we assessed combination treated mice that received FTY720 treatment or tdLN resection
287 prior to neoadjuvant therapy. TdLN resection significantly decreased the infiltration of IL-7Rα+ EM into
288 the tumor at time of resection (**Fig. 6a**) and the primary anti-tumor efficacy (**Supplementary Fig. 6a**).
289 Evaluation of memory subsets at the ndLN +30 days after primary tumor resection in mice that received
290 FTY720 during neoadjuvant treatment (**Fig. 6b**) did not affect overall CD8$^+$ T cell proportions but
291 significantly impaired TCM proportion in tumor-free mice treated with either PD-1 blockade or
292 combination therapy at day 50 (**Fig. 6c**), suggesting a critical role for lymphoid trafficking during
293 neoadjuvant therapy in establishing persistent CD8$^+$ TCM populations in ndLNs.

294 Finally, to explore memory response in long-term survivors after combination therapy, we depleted
295 different subsets of immune populations and rechallenged combination treated mice more than 30 days
296 after primary tumor resection via tail vein injection. We found that memory response did not require NK
297 cells, a known effector after IL-15Rα agonism. We also found that single depletion of $CD4^+$ or $CD8^+$ T
298 cells did not compromise tumor control. However, simultaneous depletion of both $CD4^+$ and $CD8^+$ T cell
299 populations abrogated protection (**Fig. 6d, e, supplementary Fig. 6 c, d)**. Based on these findings, we
300 investigated whether $CD4^+$ T cells were also required during tumor rechallenge in long-term responders
301 to aPD-1. We found that $CD4^+$ T cells were indeed necessary for antitumor rejection(**Supplementary Fig.**
302 **6e)**. This suggest that long-term aPD-1 responders develop an interdependent memory that requires $CD8^+$
303 and $CD4^+$ T cells for effective tumor eradication, with loss of protection upon depletion of either of these
304 subsets. These findings are consistent with more recent observations in other animal models exploring
305 aPD-1 memory[33]. Overall, our results shows that IL-15Rα relies on the tdLN for primary antitumor
306 efficacy and induces a distinct form of functional memory that differs from interdependent anti-tumor
307 efficacy observed in aPD-1 long-term responders, where only combined ablation results in loss of
308 protection from systemic rechallenge.

309

310 ***Clonal linkage mapping in early-stage NSCLC patients reveals distinct tumor draining lymph node***
311 ***$CD8^+$ T cell response following neoadjuvant PD-1 blockade***

312 To investigate the $CD8^+$ T cell compartment within tdLNs in humans, we used our groups established
313 expertise in harvesting, isolating CD8+ T cells in NSCLC patients who underwent neoadjuvant PD-1
314 blockade [34]. Surgically resected pathologically benign hilar lymph nodes (stations 11–12) from NSCLC
315 patients undergoing curative-intent lobectomy **(Fig. 7a)**. These nodes were selected based on their high

316 likelihood of draining the tumor and their frequent involvement as initial metastatic sites in regional
317 disease[35]. Flow cytometric analysis revealed an enriched population of PD-1^{+} CD8^{+} T cells within
318 tdLNs relative to peripheral blood (5–10% vs. ~2%) but markedly lower than in the tumor itself (>40%).
319 Phenotypically, tdLN-derived CD8^{+} T cells exhibited a higher frequency of effector/effector memory-like
320 subsets (CD45RA^{-}CD62L^{-}) relative to peripheral blood (30–50% vs. <20%), though this proportion
321 remained lower than in intratumoral CD8^{+} T cells (>70%) (**Fig. 7b**). Across all three compartments, the
322 majority of PD-1^{+} CD8^{+} T cells resided within the CD62L^{-}CD45RA^{-} population, suggesting a more
323 effector like phenotype.

324 Having identified a potentially tumor-reactive CD8^{+} T cell subset within tdLNs, we next investigated how
325 anatomical compartmentalization of CD8^{+} T cell responses in the tdLN influences response to aPD-1. To
326 do so, we performed paired scRNA/TCR-seq of flow sorted CD45^{+}CD3^{+}CD8^{+} T cells from matched tdLN
327 and tumor from four patients, one that did not received treatment and three patients that received
328 neoadjuvant aPD-1 plus chemotherapy of whom CM816 treatment displayed heterogenous primary tumor
329 responses. [36] (**Fig. 7c)**. One patient (WCM2050b) achieved a partial response by RECIST 1.1 criteria
330 and complete pathological response (0% RVT), one (WCM1962) exhibited stable disease (SD) by
331 RECIST, and 30% RVT at resection, another patient (WCM1906) displayed SD by RECIST, but with an
332 increase in SUV (9.8 to 14.1) prior to resection and no pathological regression (>80% RVT). Another
333 patient (WCM1906), with a comparable stage (IIb) that did not receive treatment (**Fig. 7d**). Patients were
334 clinically matched by stage and tumor PD-L1 expression of <1% [37].

335 Using previously described methodologies [24, 34, 38], we identified CD8^{+} TM expanded clones (n >9)
336 present in both the tumor and tdLN after removal of published viral epitopes. Tumor reactivity was further
337 validated using a NeoTCR score[39] and a stem-like/quiescence score[40] This confirmed that TM clones
338 in both the tumor and tdLN exhibited relatively high tumor-reactivity and low quiescence

339 (**Supplementary Fig. 7a)**. On average, each patient's TM $CD8^+$ T cell repertoire contained approximately
340 60 expanded T cell clones, except for patient WCM1927, who harbored over 90 expanded clones. UMAP-
341 based clustering of expanded TM T cells, encompassing a total of 14,464 $CD8^+$ TM T cells derived from
342 8 samples (including lymph nodes and tumors) identified nine transcriptionally distinct clusters spanning
343 a spectrum from quiescent, memory-like populations to terminally differentiated, exhausted phenotypes
344 (**Fig. 7e**). Notably, TM clones within the tdLNs were predominantly enriched within quiescent, memory-
345 like clusters (clusters 1, 2, 4, and 9) that expressed relatively higher levels of *TCF7, CCR7, SELL*, and
346 *IL7R* irrespective of treatment, and aligned with previously defined progenitor/quiescent transcriptional
347 signatures. In contrast, tumor-infiltrating clones were generally preferentially positioned in more
348 activated, effector-like, and exhausted clusters characterized by enhanced expression of cytotoxic
349 mediators (*GZMB, PRF1*) and inhibitory receptors (*TIGIT, PDCD1, HAVCR2, TOX*) recapitulating the
350 phenotype characterized in our murine model (**Supplementary Fig. 7b, c**).

351 To remove bias that may be associated with clonal dominance, we tracked individual TM clones in both
352 tissues. In tdLN TM clones were generally maintained in a more naïve- and memory-like transcriptional
353 state, often coupled with gene expression signatures favoring lymph node homing, central memory and
354 stem-like memory states. In contrast, their tumor clonal counterparts frequently acquired a cytotoxic,
355 effector, and terminally differentiated phenotype. Nevertheless, these patterns were not uniform across all
356 clones, indicating heterogeneity in differentiation trajectories (**Fig. 7f, supplementary Fig. 7d**).

357 To gain insight into the continuum of clonal differentiation states between tissues, we performed
358 pseudotime trajectory analysis[36] to reconstruct the progression of TM clones from the tdLN to the tumor
359 and assess whether intratumoral clones undergo a shift toward terminal differentiation or exhaustion. This
360 revealed a linear trajectory from a tdLN-associated, memory-like state toward a more terminally
361 differentiated, exhausted, and cytotoxic phenotype within the tumor microenvironment, characterized by

362 the loss of *TCF1*, *SELL*, and *LEF1* expression and a concomitant increase in cytotoxicity-associated
363 markers such as *GZMB*, as well as activation and markers associated with dysfunction and exhaustion
364 including *PDCD1* and *CTLA4* irrespective of treatment or pathological response (**Fig. 7g, supplementary**
365 **Fig. 7e**). Notably, this progressive effector-like differentiation was observed at the individual clone level,
366 affecting both large and small clones across multiple patients, highlighting a conserved pattern of
367 functional adaptation upon tumor infiltration.

368 Notably, although all TM $CD8^+$ T cell in the LN maintained a more memory-like cluster distribution, the
369 only pathologic complete responder (cPR) exhibited a higher representation within clusters 4 and 2,
370 showing overall the highest enrichment of *IL7R*-defined clusters within the tdLN. This pattern was also
371 reflected in the matched clones present withing the primary tumor of this patient, where there was major
372 expansion of IL7R expressing subpopulations overall. Although the partial responder also displayed an
373 expansion of cluster 2 in the tdLN, clones present in the primary tumor mostly displayed a cytotoxic
374 signature, suggesting ongoing effector activity towards residual tumor cells (**Fig. 7h)**. These findings align
375 with our mouse model data and our previous findings, where significant clonal expansion of tumor-
376 relevant clones in the tdLN of neoadjuvant-treated patients was observed compared to untreated
377 patients[34]. These findings further suggest that despite this clonal expansion, T cell differentiation within
378 the tdLN might dictate clinical responses to neoadjuvant aPD-1.

379 **Discussion**

380 Using a clinically relevant murine model of metastatic relapse following neoadjuvant PD-1 blockade and
381 surgical resection, along with clinical correlative data from NSCLC patients treated with neoadjuvant PD-
382 1 therapy, we provide a framework linking tdLN-derived progenitor cells to tumor-specific effector
383 responses and long-term immunity.

384 First, we show that tdLNs are drivers of antitumor efficacy and that aPD-1 long term survivors develop a
385 $CD8^+$ dependent memory response, with tumor relevant clones that can be found persisting in distant
386 lymph nodes. Second, our study provides direct evidence that IL-15Rα agonism in combination with
387 neoadjuvant aPD-1 promotes $CD8^+$ T cell expansion and increases clonal diversity of tumor relevant T
388 cells, changing their phenotype into effector memory precursors with increased cytotoxic features that
389 start at the tdLN level resulting in enhanced primary anti-tumor efficacy. Third, we show that after
390 treatment, IL-15 agonism promotes higher clonal persistence and lower metastatic recurrence. Finally,
391 exploration of differences in memory responses during tumor rechallenge showed that an IL-15R agonist
392 not only reprograms $CD8^+$ T cells but may also have a lasting effect in $CD4^+$ T cells. Investigation into
393 the populations required for IL-15R agonism-induced protective immunity demonstrated that while
394 neither $CD8^+$ nor $CD4^+$ T cell depletion alone compromised tumor control during rechallenge, dual
395 depletion resulted in complete abrogation of protection. These findings align with previous work exploring
396 the effect of different ICBs inducing distinct types of memory dependent on $CD4^+$ and $CD8^+$ T cells with
397 different antitumor activity[33], which demonstrates that memory can be reprogrammed for superior recall
398 responses. Our work suggests that IL-15 impacts both T cell populations to induce robust antitumor
399 memory and motivates future phenotypic characterization of memory and functional features in $CD4^+$ T
400 cells.

401 Our results align with a growing body of evidence showing that the efficacy of PD-1 ICB relies on a
402 progenitor-like T cell subset for long-term maintenance of T cell responses[41], and that tdLNs are a
403 reservoir of tumor specific $CD8^+$ T cells[42] that are precursors of T cells in the tumor [43] maintained
404 by continuous migration from the lymph node[3, 4]. With surgical resection of tdLNs resulting in loss of
405 therapy-induced tumor regression[44]. This suggest that PD-1 blockade in the surgical setting for NSCLC
406 requires special considerations, as regional benign hilar and mediastinal are routinely resected as part of

407 standard surgical management—often before or during immunotherapy—despite their potential role in
408 sustaining systemic antitumor immunity.

409 IL-15 immunomodulation has emerged as a safe and potent strategy to enhance endogenous anti-tumor
410 immunity. The phase I clinical trial of KD033 in patients with metastatic and locally advanced disease
411 (NCT04242147) reported no dose-limiting toxicities and remains ongoing[45]. The IL-15 superagonist
412 N-803 now FDA-approved for BCG-unresponsive early-stage bladder cancer, achieved a complete
413 response in 71% of patients through direct activation of $CD8^+$ T cells[46]. It is currently under active
414 investigation in ICB refractory advanced-stage NSCLC in combination with PD-1 blockade. To date, IL-
415 15Rα agonism has not been tested in the neoadjuvant setting . Here, we show that combining an IL-15R
416 agonist with PD-1 blockade elicits potent tumor-directed cytolytic activity and sustains long-lived, tumor-
417 specific T cells whose generation depends on the tumor-draining lymph node. These findings provide a
418 strong rationale for neoadjuvant IL-15/PD-1 combination strategy to achieve durable clinical benefit,
419 forming the basis for our planned phase II clinical trial in early-stage NSCLC.

420 **Materials and methods**

421 Animal work

422 Animal work was performed in accordance with an animal protocol approved by the institutional Animal
423 Care and Use Committee at Weill Cornell Medical College (protocol no. 0806-762A). Female 129SvlmJ
424 were purchased from the Jackson Laboratory (Cat.No 002448).

425 Culturing of cell lines

426 344SQ lung cancer cell line was kindly provided from Dr. Jonathan Kurie's lab (MD Anderson Cancer
427 Center, Houston, TX). Tumor cells were obtained from subcutaneous tumors from *p53*$^{R172H\Delta g/+}$ *K-*

428 *ras*$^{LA1/+}$ mice. These cells were cultured in DMEM supplemented with 10% FBS, L-glutamine 10mM and
429 100 U ml^{-1} penicillin with 100 μg ml^{-1} streptomycin. mCherry-luciferase stable expression was achieved
430 using lentiviral transduction.

431 Flank injection of tumor cells in syngeneic (129SvlmJ)

432 We used immune-competent 129Sv (Jackson Laboratory, Bar Harbor, ME USA 04609) female thar were
433 at least 8-12 weeks old for our *in vivo* studies. 1e^{6} 344SQ expressing mCherry-luciferase cells were
434 harvested at 50-70% confluence and resuspended in 100 ul of PBS and injected in the right flank. Tumor
435 growth in vivo was evaluated at day 3 after injection and once weekly via BLI using a Xenogen IVIS
436 system. To cohort mice for different treatments BLI data was collected 1 day before treatment and mice
437 were group such that similar mean tumor burden was present in each group. All treatment groups started
438 therapy after 3 weeks of tumor growth on same day. For treatment with aPD-1 or IgG2a mice were injected
439 intraperitoneally with 250ug of anti-PD-1 or IgG2a as previously reported[15] on days 1,4,7 of treatment.
440 Mice treated with IL-15 superagonist (KD033) received a single dose by tail vein injection (3mg/kg) at
441 same time of first dose of aPD-1. Mice that received combination therapy received IL-15 superagonist
442 single dose at day 1 of treatment and aPD-1, two additional doses of aPD-1 on days 4 and 7 of treatment.
443 3 days after last dose of treatment all mice underwent survival surgery at the same time.

444 For FTY720 experiments, FTY720 was resuspended in saline at a concentration of 30ug in 100 ul through
445 IP injection starting 2 or 6 days prior first dose of aPD-1 and was continued every other day during
446 treatment and until surgical resection timepoint. After this mouse were follow and posteriorly ntdLN
447 (contralateral, left inguinal) was resected more than 30 days after primary tumor resection for phenotyping.
448 FTY 720 depletion was confirmed by flow cytometry of blood from jawbleeds.

449 For depletion studies matched cohorts of mice that underwent different neoadjuvant treatments and
450 completed at least 30 days after survival surgery received CD4,CD8 and/or NK depleting antibodies
451 depending on the depletion group with the following doses: 400 µg anti-CD4 (clone GK1.5, BioXCell),
452 400 µg anti-CD8a (clone 2.43, BioXCell), and 50 ul of anti asialo antibody (GM1). Respective controls
453 were also used depending on the depletion group compensating for antibody load in respective groups.
454 For rechallenge experiments 700.000 344sq Mcherry expressing cells were injected through tail vein
455 injection. Efficacy of depleting antibodies was confirmed by flow cytometry of blood from jaw bleeds.

456 Survival surgery

457 The animals were anesthetized utilizing isoflurane. An injection of buprenorphine extended release
458 (Ethiqa XR) SC was given for pre-emptive analgesia immediately after the animal were anesthetized.
459 Depth of anesthesia was monitored at least every 15 minutes throughout the procedure. Following
460 confirmation that a suitable anesthetic plane was attained, sterile eye lubricant was applied to both eyes to
461 prevent corneal drying during surgery, alternative scrubs of ethanol 70% and chlorhexidine were given 3
462 times in the area for surgical incision. Animals were covered with a sterile drape with a hole for access to
463 the incision and kept warm using a heating pad. Fresh sharp scissors were used to make an incision size
464 of up to twice the diameter of the tumor through the skin directly overlaying the mass. Sterile hemostats
465 were used to bluntly dissect the tumor and or tdLN (inguinal) away from the underlying normal tissue.
466 During blunt dissection, blood vessels feeding or draining the tumor were ligated. Once the tumor was
467 separated from the surrounding tissue, it was carefully removed using sterile forceps for grasping the mass
468 and sterile scissors to facilitate removal. Skin edges were apposed and closed with sterile wound clips.
469 Mice were monitored during recovery from anesthesia and were follow up twice at 24-, 48- and 72-hour
470 timepoints for signs of post-surgical complications or pain and treated accordingly to protocol. Sutures
471 were removed between day 7 and day 14.

472 Mouse tissue harvest

473 At specific timepoints tissues were collected during survival surgery, kept on supplemented culture media
474 at 4 °C, then tumors were ground through a 140 -µm wire mesh (Cell Screen/100mesh, Bellco Glass) then
475 filtered through 70-µm filters. Lymph nodes were dissected and filtered through 70-µm filters. Red blood
476 cell lysis into single cell suspension was achieved by using ACK lysing Buffer and cell pellets were
477 washed and resuspended in FACS buffer.

478 Flow cytometry staining

479 For surface staining samples were incubated with a fixable live/dead viability dye (Zombie Aqua,
480 BioLegend), stained with primary antibodies in the presence of Fc blockers, washed with FACS buffer,
481 fixed with 1% formaldehyde, washed with FACS buffer and resuspended in FACS buffer.

482 Transcription factor staining: Samples were incubated with Zombie Aqua fixable live/dead dye, stained
483 with primary antibodies in the presence of Fc blockers, washed with FACS buffer, fixed with
484 Fixation/Permeabilization Buffer (eBioscience), washed with Permeabilization Buffer (eBioscience),
485 stained with primary antibodies for intracellular markers in Permeabilization Buffer, washed with
486 Permeabilization Buffer and resuspended in FACS buffer.

487 Cytokine staining: Single cell suspension obtained after ACK lysis buffer was incubated a 37 °C in a
488 humidified incubator for 5 hours using golgi blockers brefeldin A (Biolegend) and monensin (Biolegend),
489 and cytokine stimulants PMA and Ionomycin. After incubation cells were stained for surface and
490 intracellular markers as described above.

491

492 Sorting of T cells for single cell TCR sequencing analysis.

493 At specific timepoints tissues were collected during survival surgery, kept on supplemented culture media
494 at 4 °C, tissues were collected, processed and ACK lysed as described above, single cell suspension was
495 stained using primary antibodies in the presence of Fc blockers, washed and resuspended in FACS buffer
496 and stained with CD3, CD8, CD45, CD62L and CD45RA (Human samples) or CD44 (mouse
497 experiments) and DAPI 0.2 ug ml^{-1}. Sorting strategy used was CD45+,CD3+,CD8+, CD62L+ and
498 CD45RA/CD44 was used to verify phenotypes during sorting.

499 Patient sample collection and use

500 All patient specimens were collected following consent from the Cardiothoracic Surgery Department,
501 Weill Cornell Medical College. Specimens were collected after obtaining written informed consent before
502 undergoing any study-specific procedures in accordance with the Declaration of Helsinki. Patient identity
503 for pathological specimens remained anonymous in the context of this study. Patient sample collection
504 was approved by the institutional review board of Weill Cornell Medical College: Thoracic Surgery
505 Biobank protocol no. 23-04025976.

506 scRNASeq and scTCRSeq and demultiplexing and read processing

507 To align raw single cell RNA Seqeuncing and single cell V(D)J sequencing data we used Cell Ranger
508 version 3.0.2 multi. The GEX mm10-2020-A mouse reference genome was used for transcriptional
509 reference along with GRCm38 mouse reference for V(D)J. Aligned transcriptional data is the processed
510 using Read10X using R version 3.6.1. Seurat version 3 was used to create a seurat object with the
511 following parameters: min.cells set to 3 and min.features parameter set to 200. TCR V(D)J data was then
512 processed by combining the filtered_contig_annotations.csv and clonotypes.csv dataset to get the cdr3
513 alpha and beta amino acid sequence for each cell, which was then added as meta data to the Seurat object.

514 Single-cell TCR sequencing quality control and clonal analysis

515 CD8 T cells were filtered to have at least both one α and one β chain sequenced. Distinct TCR clones were
516 determined by the exact combination of α and one β chain amino acid sequences. Clone size was then
517 calculated as the number of cells within the same TCR α and one β chain sequenced. Only expanded
518 clones, clones with at least three cells as mentioned in literature, were used in all downstream clonal
519 analysis. Clones were categorized into two categories of clonal matching: non-tissue-matched (non-tm)
520 and tissue-matched (tm). If all cells within a clone were found in single tissue it was denoted as non-tm.
521 If a clone in the tdLN had a paired TCR clone found in the tumor, it was categorized as tissue matched
522 (tm) clone. Persisting clones, a subcategory of tm clones, were categorized as clones with T cells found
523 in both tdLN and tumor and then also in the ndLN after tumor resection. Each T cell was labeled as being
524 part of a non-tm or tm clone as well as the clone ID. After unexpanded clones were removed, the clonality
525 of a tissue for each treatment was analyzed in three ways: clonal diversity, the percent of total tm T cell,
526 and a normalized weighted expansion score. The clonal diversity of a group was calculated to be the total
527 number of clones within that group.

528 For patient samples to reduce likelihood of tumor bystander T cells, extra filtering steps were taken. The
529 https://vdjdb.cdr3.net/ antigen-specific TCR amino acid sequence data base was then used to determine
530 viral clones. These clones were then filtered out. Following this, unexpanded clones (n<10) were also
531 filtered out. To validate our methods of reducing by standing CD8 T cells, we applied a tumor-reactive
532 signature from the literature, comparing non-tm cells, tm viral, non-viral unexpanded tm cells, and
533 expanded tm cells within the tdLN and tumor.

534 Single-cell RNA computational processing

535 ScRNA sequencing data was preprocessed following the steps instructed by the Seurat tutorial vignettes.
536 All cells with a percentage of mitochondrial genes, high or low number of features, were removed as

quality control. Cell's transcriptional data was normalized by using Seurat's *NormalizeData* with the LogNormalized method and a scale factor of 10000. The 2000 most variable features, as suggested by Seurat, were found via *FindVariableFeatures* using the vst method. PCA's were calculated using the *runPCA* function. The number of dimensions used in *RunUMAP* was based on the elbow plot of PCA dimensions. To remove non-CD8 T cell from the dataset, all cells without TCR sequencing were removed. In addition, cell expression for CD8 and Cd3 (*Cd3g, Cd3e, Cd3d, Cd8a, Cd8b, Cd8b2*) was tested. Common cell types that were also filtered were epithelial cells, B cells, CD4 T+ CD8- T cells, although after removed cells without TCR sequencing the need to remove other cell types minimized. Meta data about each of the mouse's treatment, response, and recurrence status was also added and later used for differential expression to compare functional changes.

Two mice cohort experiments were sequenced and were integrated by cohort to remove sequencing bias. Cells were integrated using *RunHarmoney* based on cohort to remove any cohort-specific or sequence-specific bias. When analysis was preformed to directly compare experiments, a new Seurat object with all samples was created and clustered using the same preprocessing and clustering procedure. T cells from sequenced mice had ndLN resected 30 days after initial resection to trace TCR clone longitudinally. Mice that did not recure or die by the 30 days after initial tumor resection were selected and persisting clones were determined by tracing which tm clones were also found in the ndLN. A new UMAP was then generated using persisting clones.

Patient samples were integrated using *RunHarmoney* based on patient ID to remove any patient-specific or sequence-specific bias.

Transcriptional signature analysis with TCR clonal matching category

558 To compare T cell functionality between TCR matching groups, relative functional scores were generated
559 using Seurat's *addModuleScore*, which were then centered and scaled. Markers to create scores were
560 taking from literature. For example, *Sell, Tcf7, Ccr7, Il7r, S1pr1,* and *Klf2* are naïve and central memory
561 positive markers described by Pauken et al. based on Pauken et al, an effector and effector memory gene
562 score included *Klrg1, Cx3cr1, S1pr5, Tnf, Ifng, Gzmb,* and *Prf1*. A cytotoxic score was generated by
563 combining known cytotoxic genes *Prf1, Ifng, Nkg7, Gzmb, Gzma, Gzmm, Klrk1, Klrb1a, Klrb1c, Klrd1,*
564 *Ctsw,* and *Cst7[24].* The migration score was determined from Hashimoto et al to include *Cxcr3, S1pr1,*
565 *Klf2, Itgb1, Cd44,* and *Ly6c2[7]*.

566 Scores were then compared between meta data (matching category, tissue, treatment, recurrence, etc.) or
567 a combination of meta data by using boxplots and statistically compared using t test. To determine how
568 tissue and treatment affect T cell subtypes, proportion of Seurat cluster distributions were created using
569 *ggplot*. Lastly, in order to understand how T cell relative function changes within a clone in different
570 tissues and presence of antigen, functional scores were averaged per tissue per clone. Each clonal average
571 was then plotted using *geom_point* and each clone was followed via a connected line. Clones were colored
572 based on tissue and a paired T-test was used to determine changes. To compare functional score and gene
573 changes across all mice, tissues, and scores, each score was transformed into a Z-score, where the average
574 was zero and the standard deviation was one. Differential expression was preformed using *FindMarkers*
575 or *FindAllMarkers* to determine changes between clusters, tissues, or treatments, where min.pct and
576 logfc.threshld were 0.25. *EnhancedVolcano* plot was used to demonstrate the differentially expressed
577 genes, with a pCutOff of 0.05 and FCcutoff of 0.5.

578 Single-cell RNA pseudotime analysis

Monocle3 was used to perform a pseudotime analysis to study persistant clone-specific and treatment-specific T cell trajectories. T cells were first filtered to include only persisting clones. A new UMAP was created in Seurat to classify T cell subtypes using the functional annotations, differential expression using *FindAllMarkers*, and functional scores using *addmodulescore*. The Seurat object along with its metadata was then converted to a large cell_data_set object. This object was then preprocessed, aligned by cohort and then *reduce_dimensions* was run, as suggested by Monocle3. Following this method, *cluster_cells* was used using the Louvain method, and the a trajectory was determined via *learn_graph*. The earliest principal node was determined by the earliest principal node in the tdLN. The location of the earliest principal node was then check with biological standards of known less differentiated markers. The pseudotime trajectory was then compared with previously annotate T cell subtypes, tissue type, and functional scores.

References

1. Lee, A.H., et al., *Neoadjuvant PD-1 blockade induces T cell and cDC1 activation but fails to overcome the immunosuppressive tumor associated macrophages in recurrent glioblastoma.* Nature Communications, 2021. **12**(1).
2. Im, S.J., et al., *Defining CD8+ T cells that provide the proliferative burst after PD-1 therapy.* Nature, 2016. **537**(7620): p. 417-421.
3. Connolly, K.A., et al., *A reservoir of stem-like CD8 ⁺ T cells in the tumor-draining lymph node preserves the ongoing antitumor immune response.* Science Immunology, 2021. **6**(64).
4. Prokhnevska, N., et al., *CD8+ T cell activation in cancer comprises an initial activation phase in lymph nodes followed by effector differentiation within the tumor.* Immunity, 2023. **56**(1): p. 107-124.e5.
5. Dammeijer, F., et al., *The PD-1/PD-L1-Checkpoint Restrains T cell Immunity in Tumor-Draining Lymph Nodes.* Cancer Cell, 2020. **38**(5): p. 685-700.e8.
6. Forde, P.M., et al., *Overall Survival with Neoadjuvant Nivolumab plus Chemotherapy in Lung Cancer.* New England Journal of Medicine, 2025.
7. Hashimoto, M., et al., *PD-1 combination therapy with IL-2 modifies CD8+ T cell exhaustion program.* Nature, 2022. **610**(7930): p. 173-181.
8. Rochman, Y., R. Spolski, and W.J. Leonard, *New insights into the regulation of T cells by γc family cytokines.* Nature Reviews Immunology, 2009. **9**(7): p. 480-490.
9. Waldmann, T.A., *The Shared and Contrasting Roles of IL2 and IL15 in the Life and Death of Normal and Neoplastic Lymphocytes: Implications for Cancer Therapy.* Cancer Immunology Research, 2015. **3**(3): p. 219-227.
10. Yang, Y. and A. Lundqvist, *Immunomodulatory Effects of IL-2 and IL-15; Implications for Cancer Immunotherapy.* Cancers, 2020. **12**(12): p. 3586.
11. Lee, J., et al., *IL-15 promotes self-renewal of progenitor exhausted CD8 T cells during persistent antigenic stimulation.* Frontiers in Immunology, 2023. **14**.
12. Gibbons, D.L., et al., *Contextual extracellular cues promote tumor cell EMT and metastasis by regulating miR-200 family expression.* Genes & Development, 2009. **23**(18): p. 2140-2151.
13. Knopf, P., et al., *Preclinical Identification Of Tumor-Draining Lymph Nodes Using a Multimodal Non-invasive In vivo Imaging Approach.* Molecular Imaging and Biology, 2023. **25**(3): p. 606-618.
14. Horton, B.L., et al., *Lack of CD8 ⁺ T cell effector differentiation during priming mediates checkpoint blockade resistance in non–small cell lung cancer.* Science Immunology, 2021. **6**(64).
15. Markowitz, G.J., et al., *Immune reprogramming via PD-1 inhibition enhances early-stage lung cancer survival.* JCI Insight, 2018. **3**(13).
16. Oh, M.S., et al., *Tumor Heterogeneity and the Immune Response in Non-Small Cell Lung Cancer: Emerging Insights and Implications for Immunotherapy.* Cancers, 2025. **17**(6): p. 1027.
17. Micevic, G., et al., *IL-7R licenses a population of epigenetically poised memory CD8 ⁺ T cells with superior antitumor efficacy that are critical for melanoma memory.* Proceedings of the National Academy of Sciences, 2023. **120**(30).
18. Herndler-Brandstetter, D., et al., *KLRG1+ Effector CD8+ T Cells Lose KLRG1, Differentiate into All Memory T Cell Lineages, and Convey Enhanced Protective Immunity.* Immunity, 2018. **48**(4): p. 716-729.e8.
19. Hänninen, A., et al., *Ly6C supports preferential homing of central memory CD8⁺ T cells into lymph nodes.* European Journal of Immunology, 2011. **41**(3): p. 634-644.
20. Williams, B.A., et al., *Predicting Postrecurrence Survival Among Completely Resected Nonsmall-Cell Lung Cancer Patients.* The Annals of Thoracic Surgery, 2006. **81**(3): p. 1021-1027.
21. Boersma, B., H. Poinot, and A. Pommier, *Stimulating the Antitumor Immune Response Using Immunocytokines: A Preclinical and Clinical Overview.* Pharmaceutics, 2024. **16**(8): p. 974.

22. Lee, H., S.-H. Park, and E.-C. Shin, *IL-15 in T-Cell Responses and Immunopathogenesis.* Immune Network, 2024. **24**(1).
23. Martomo, S.A., et al., *Single-Dose Anti–PD-L1/IL-15 Fusion Protein KD033 Generates Synergistic Antitumor Immunity with Robust Tumor-Immune Gene Signatures and Memory Responses.* Molecular Cancer Therapeutics, 2021. **20**(2): p. 347-356.
24. Pauken, K.E., et al., *Single-cell analyses identify circulating anti-tumor CD8 T cells and markers for their enrichment.* Journal of Experimental Medicine, 2021. **218**(4).
25. Andreatta, M., et al., *Interpretation of T cell states from single-cell transcriptomics data using reference atlases.* Nature Communications, 2021. **12**(1).
26. Ayers, M., et al., *IFN-γ–related mRNA profile predicts clinical response to PD-1 blockade.* Journal of Clinical Investigation, 2017. **127**(8): p. 2930-2940.
27. Miller, B.C., et al., *Subsets of exhausted CD8+ T cells differentially mediate tumor control and respond to checkpoint blockade.* Nature Immunology, 2019. **20**(3): p. 326-336.
28. Kaech, S.M., et al., *Molecular and Functional Profiling of Memory CD8 T Cell Differentiation.* Cell, 2002. **111**(6): p. 837-851.
29. Doering, T.A., et al., *Network Analysis Reveals Centrally Connected Genes and Pathways Involved in CD8+ T Cell Exhaustion versus Memory.* Immunity, 2012. **37**(6).
30. Chihara, N., et al., *Induction and transcriptional regulation of the co-inhibitory gene module in T cells.* Nature, 2018. **558**(https://doi.org/10.1038/s41586-018-0206-z).
31. Tsyklauri, O., et al., *Regulatory T cells suppress the formation of potent KLRK1 and IL-7R expressing effector CD8 T cells by limiting IL-2.* Elife, 2023.
32. Yao, C., et al., *Single-cell RNA-seq reveals TOX as a key regulator of CD8+ T cell persistence in chronic infection.* Nature Immunology, 2019. **20**(7): p. 890-901.
33. Mok, S., et al., *Anti-CTLA-4 generates greater memory response than anti-PD-1 via TCF-1.* Proceedings of the National Academy of Sciences, 2025. **122**(2).
34. Honigsberg, R., et al., *Tumor-specific draining lymph node CD8 T cells orchestrate an anti-tumor response to neoadjuvant PD-1 immune checkpoint blockade*. 2025, Cold Spring Harbor Laboratory.
35. Gilmore, D.M., et al., *Identification of metastatic nodal disease in a phase 1 dose-escalation trial of intraoperative sentinel lymph node mapping in non–small cell lung cancer using near-infrared imaging.* The Journal of Thoracic and Cardiovascular Surgery, 2013. **146**(3): p. 562-570.
36. Hou, W., et al., *A statistical framework for differential pseudotime analysis with multiple single-cell RNA-seq samples.* Nature Communications, 2023. **14**(1).
37. Forde, P.M., et al., *Neoadjuvant Nivolumab plus Chemotherapy in Resectable Lung Cancer.* New England Journal of Medicine, 2022. **386**(21): p. 1973-1985.
38. Szabo, P.A., et al., *Single-cell transcriptomics of human T cells reveals tissue and activation signatures in health and disease.* Nature Communications, 2019. **10**(1).
39. Lowery, F.J., et al., *Molecular signatures of antitumor neoantigen-reactive T cells from metastatic human cancers.* Science, 2022. **375**(6583): p. 877-884.
40. Krishna, S., et al., *Stem-like CD8 T cells mediate response of adoptive cell immunotherapy against human cancer.* Science, 2020. **370**(6522): p. 1328-1334.
41. Siddiqui, I., et al., *Intratumoral Tcf1+PD-1+CD8+ T Cells with Stem-like Properties Promote Tumor Control in Response to Vaccination and Checkpoint Blockade Immunotherapy.* Immunity, 2019. **50**(1): p. 195-211.e10.
42. Liu, Q., et al., *Tumor-specific memory CD8+ T cells are strictly resident in draining lymph nodes during tumorigenesis.* Cellular & Molecular Immunology, 2023. **20**(4): p. 423-426.
43. Rahim, M.K., et al., *Dynamic CD8+ T cell responses to cancer immunotherapy in human regional lymph nodes are disrupted in metastatic lymph nodes.* Cell, 2023. **186**(6): p. 1127-1143.e18.
44. Fransen, M.F., et al., *Tumor-draining lymph nodes are pivotal in PD-1/PD-L1 checkpoint therapy.* JCI Insight, 2018. **3**(23).

45. Luke, J.J., et al., *Phase I dose escalation of KD033, a PDL1-IL15 bispecific molecule, in advanced solid tumors.* JOURNAL OF CLINICAL ONCOLOGY, 2021. **39**.
46. Chamie, K., et al., *Final clinical results of pivotal trial of IL-15RαFc superagonist N-803 with BCG in BCG-unresponsive CIS and papillary nonmuscle-invasive bladder cancer (NMIBC).* JOURNAL OF CLINICAL ONCOLOGY, 2022. **40**.
47. Ciecko, A.E., et al., *Self-Renewing Islet TCF1+ CD8 T Cells Undergo IL-27–Controlled Differentiation to Become TCF1− Terminal Effectors during the Progression of Type 1 Diabetes.* The Journal of Immunology, 2021. **207**(8): p. 1990-2004.
48. Wang, C., et al., *Clinicopathological variables influencing overall survival, recurrence and post-recurrence survival in resected stage I non-small-cell lung cancer.* BMC Cancer, 2020. **20**(1).
49. Zhang, S., et al., *Immunosequencing identifies signatures of T cell responses for early detection of nasopharyngeal carcinoma.* Cancer Cell, 2025.
50. Li, H., et al., *Distinct CD8+ T cell dynamics associate with response to neoadjuvant cancer immunotherapies.* Cancer Cell, 2025. **43**(4): p. 757-775.
51. Galletti, G., et al., *Two subsets of stem-like CD8+ memory T cell progenitors with distinct fate commitments in humans.* Nature Immunology, 2020. **21**(12): p. 1552-1562.
52. Tsui, C., et al., *MYB orchestrates T cell exhaustion and response to checkpoint inhibition.* 2022.
53. Yossef, R., et al., *Phenotypic signatures of circulating neoantigen-reactive CD8+ T cells in patients with metastatic cancers.* cancer cell, 2023. **41**: p. 2154–2165.

Acknowledgements: We thank J. McCormick, T. Baumgartner, P. Byrne and M. Romero of the Flow Cytometry Core Facility, J. Xiang of the Genomics Resources Core Facility. We thank P. Adusumilli or helpful discussions and critical manuscript review. We thank S. B. Lee for animal colony management.

Author contribution: T.D.C. and J.V.V conceptualized the project and designed the experiments. T.D.C. performed the mouse experiments with A.S. and M.T. assistance. R.H. performed single cell sequence data analysis and interpretated the data along J.V., T.D.C. and O.E., V.M. and N.K.A. provided project oversight and support. T.D.C. and J.V.V wrote the manuscript. T.D.C. and J.V.V edited the manuscript with input from the authors. All authors discussed the results and conclusions drawn from the studies.

Competing interests: Authors have declared no financial or other competing interest.

Data and materials availability: All data, code, and materials used in the analysis were sourced from common established methodologies and publicly available packages on R. We described the pipeline of

the analysis in the methods section and have affirmed that the code is available to readers upon reasonable request.

Fig. 1. Surgical murine model displays tdLN CD8^{+} T cell dependent response to neoadjuvant aPD-1.

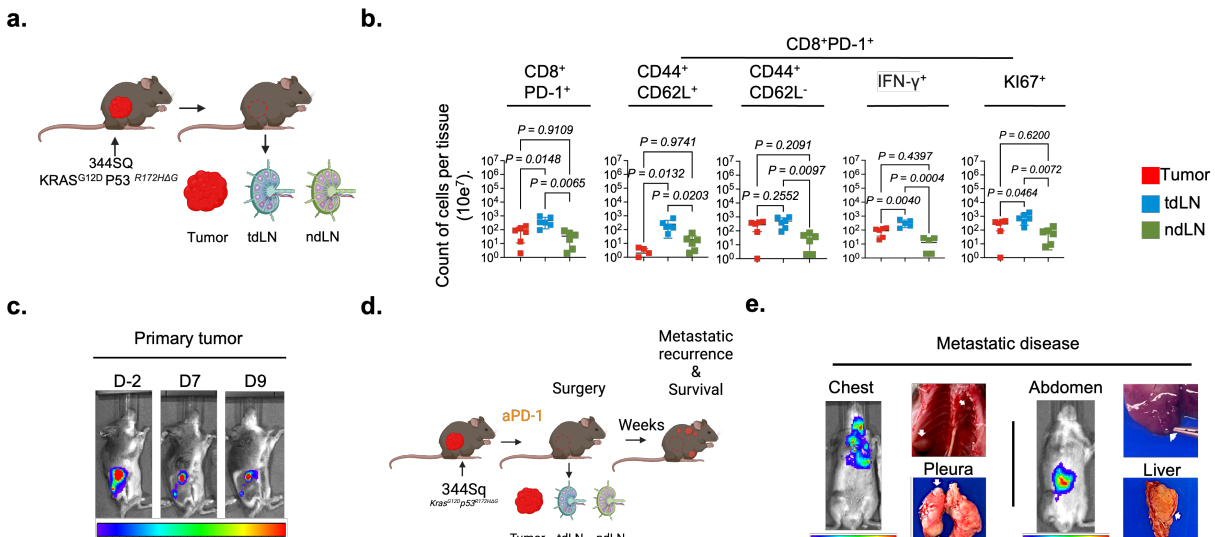

745

746

747

748

749

750

751

752

753

754

755

756

757

758 **Fig. 1.** Surgical murine model displays tdLN $CD8^+$ T cell dependent response to neoadjuvant aPD-1. **a.**
759 Experimental design for tumor, tumor draining lymph node (tdLN) and non-tumor draining lymph node
760 (ndLN) characterization, **b.** Flow cytometry quantification of $CD8^+$ T cells in tumor, tdLN and ndLN,
761 showing counts of $CD8^+PD\text{-}1^+$ T cells, memory subpopulations determined by CD44 and CD62L
762 expression, IFNγ and KI67 expression between tissues was also evaluated (total of 6 biological replicates
763 per tissue *(n=6))*, **c.** representative bioluminescence (BLI) images of flank tumor burden of an aPD-1

responder mouse on days -2,7,9 of treatment, **d.** Experimental design of neoadjuvant experiments using aPD-1, **e.** Representative bioluminescence images and necropsy pictures of metastatic disease developed after primary tumor resection showing common sites of metastasis, **f.** Schematic for FTY720 experiments, **g.** BLI plots of tumor growth kinetics during treatment with IgG control (gray), aPD-1 (orange) and aPD-1+FTY720 (denoted by black arrow), **h.** Flow cytometry quantification of $CD8^+$ T cell populations in the tumor and tdLN of mice receiving aPD-1 or aPD-1+FTY720, **i.** Overall survival of mice treated with aPD-1 or IgG, **j.** Kaplan Meier survival plots of mice that develop recurrence (dotted line) VS no recurrence (long term responders), **k.** Experimental design of rechallenge/depletion experiments, **l.** BLI plots of tumor burden of tumor rechallenge of long-term responders receiving CD8 depletion (red), IgG control (orange) or naïve age match mice (black), **m.** Kaplan Meier survival plots for experimental groups in depletion experiment. Statistics used were one-way analysis of variance (ANOVA) **(b.) (h.)**, log-rank Mantel–Cox test **(i.)(m.)**.

Fig. 2. Neoadjuvant IL-15Rα agonist in combination with PD-1 blockade displays robust efficacy in primary tumor and protection from metastatic relapse.

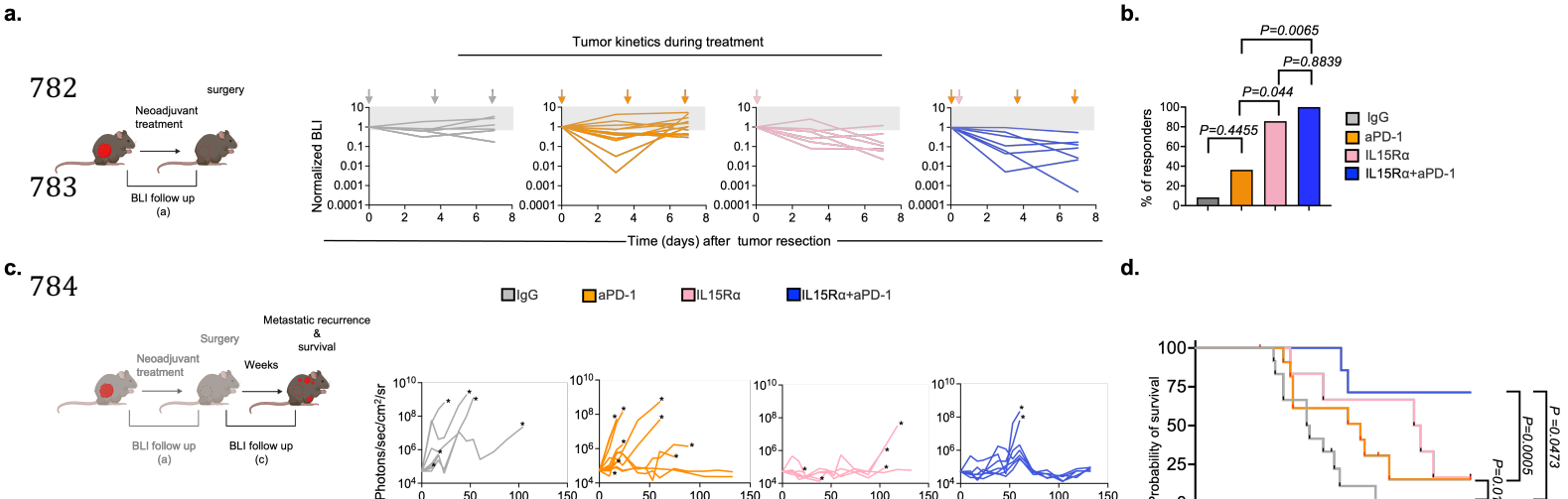

785

786

787

788

789

790

791

792

793

794

795

796

797 **Fig. 2.** Neoadjuvant IL-15Rα agonist in combination with PD-1 blockade displays robust efficacy in
798 primary tumor and protection from metastatic relapse. **a.** Schematic of experimental design (left) and BLI
799 plots of primary tumor burden kinetics during treatment with IgG (gray), aPD-1 (orange),IL15Rα (pink)
800 or aPD-1+IL15Rα (blue), **b.** Quantification of responder mice per treatment n=6-13 per
801 group, **c.** Schematic design of recurrence follow up showing past experimental timepoints until surgery in
802 gray (left) and BLI plots of metastatic disease after primary tumor resection (right), asterisks denote
803 mortality during follow up, **d.** Kaplan Meier survival plots of mice from different treatments after primary

tumor resection up to 200 days. Statistics used were one Way ANOVA **(b.)**, and siddaks log-rank Mantel–Cox test **(d.)**.

Fig. 3. IL-15Rα directs tdLN CD8+ clones towards an IL-7R α effector memory subset.

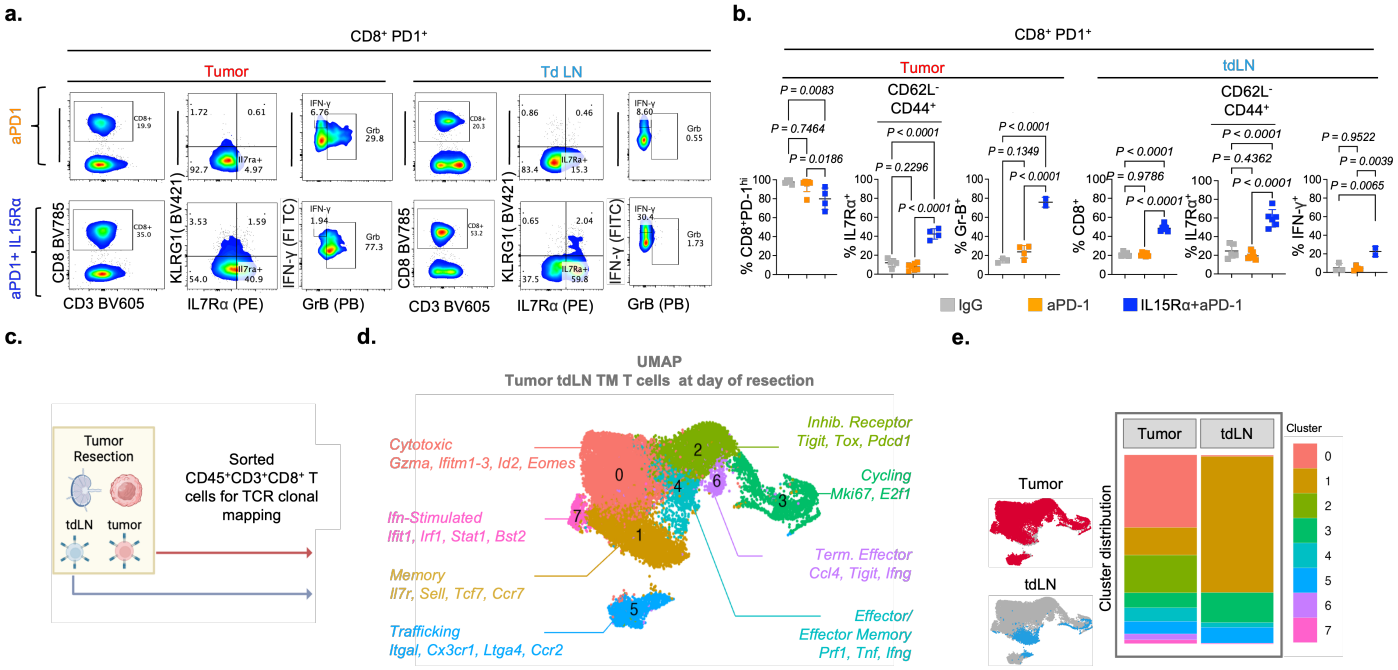

822

823

824

825

826

827

828

829

830

831

832

833 **Fig. 3.** IL-15Rα directs tdLN CD8+ clones towards an IL-7R α effector memory subset. **a.** Representative
834 flow cytometry plots of $CD8^+$ T cells from tumor and tdLNs resected at time of survival surgery timepoint
835 from mice treated with aPD-1 or aPD-1+IL-15Rα for the expression of KLRG1,IL7Rα, interferon gamma
836 (Ifnγ) and Granzyme b (Grb), **b.** Flow cytometry quantification of $CD8^+$ T cell subsets for experiment in
837 b. *(n= 3-5 per group),* **c.** Experimental design for single cell RNA sequencing (scRNAseq) experiments,
838 **d.** Clustering and UMAP visualization of CD8 tumor match (TM) clones from tumor and tdLNs at day of
839 surgical resection *(n=249 clones)* integrated from 9 mice from two different experiments, color denote
840 transcriptional clusters, labeled with functional annotations, **e.** UMAP showing cluster distribution of

tumor match clones from tumor and tdLN (left), and cluster distribution for each cluster in figure 4e. in respective tissues (right), **f.** UMAP showing relative expression of naïve/central memory (CM)Pauken, Shahid [24], terminal differentiation (Term. Diff) Ciecko, Schauder [47], activation & migration Wang, Wu [48] and cytotoxic gene signatures Zhang, Zhou [49], **g.** UMAP showing clone distribution per treatment, **h.** Cluster distribution for each cluster in figure 4e. per treatment and tissue, **i.** Heatmap for genes grouped by function (Memory, dysfunctional, cytotoxic/effector, migration & adhesion, co-stimulation (Co-Stim) and AP-1) and Z score average by tissue and treatment for each gene. Statistics used were one way ANOVA **(b.).**

Fig. 4. Il-15Rα induced IL-7R α effector memory CD8^{+} T cell differentiation begins in the tdLN.

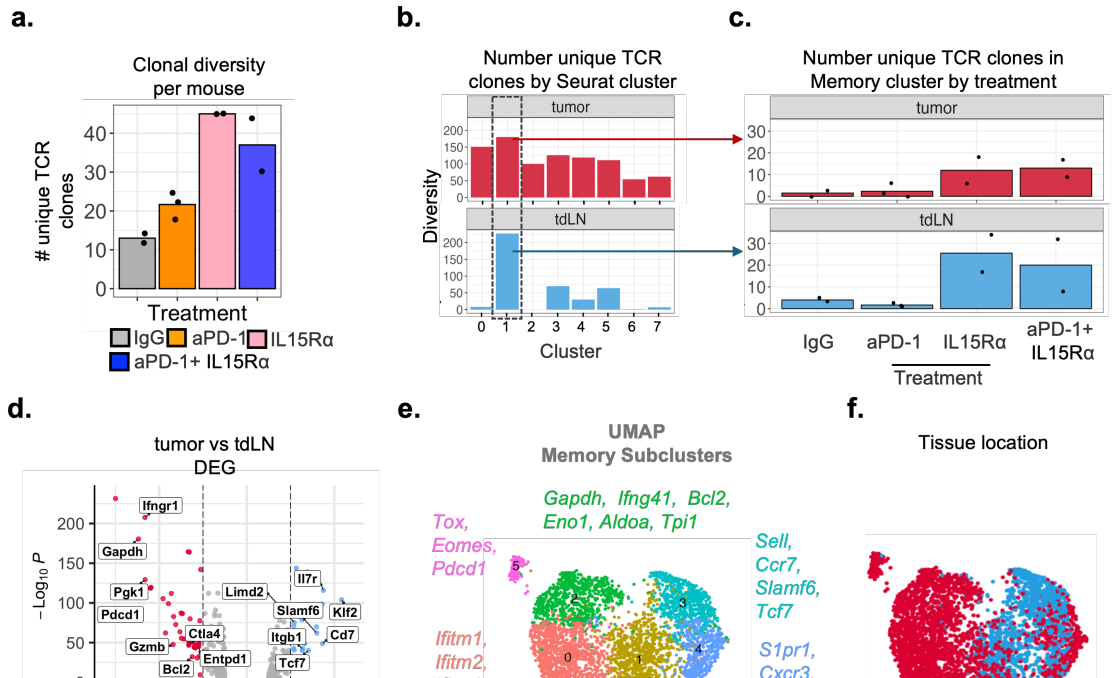

860

861

862

863

864

865

866

867

868

869

870

871 **Fig. 4.** Il-15Rα induced IL-7Rα effector memory $CD8^+$ T cell differentiation begins in the tdLN. **a.**
872 Quantification of number of unique TCR clones per mouse and treatment, each dot represents one mouse
873 *(n=9)*, **b.** Bar plots showing clonal diversity in the tumor (top) and the tumor draining lymph node(bottom)
874 per cluster depicted in figure 4.e, **c.** Number of unique TCR clones in memory cluster (cluster 1) per
875 treatment in tumor (top) and tumor draining lymph node (bottom), **d.** Volcano plot of differentially
876 expressed genes between tumor and tdLN T cells in cluster 1, **e.** UMAP of memory subclusters from
877 memory cluster 1 in figure 4e., labeled by top genes within the cluster, **f.** UMAP showing distribution of
878 tumor (red) and tdLN (blue) T cell clones on memory subclusters, **g.** Volcano plot of differentially

expressed genes of tdLN memory T cells from mice treated with aPD-1 Vs aPD-1+IL15Rα, **h.** Clone distribution in memory subclusters by treatment, **i.** Bar plots showing cluster distribution in memory subclusters by tissue and treatment, **j.** Z score for KILR Effector Tsyklauri, Chadimova [31] and progenitor Yao, Sun [32] signature for clones in tumor and tdLN from different treatments. Statistics used were t-test **(j.)**.

\

Fig. 5. CD8^{+} T cell clonal response in tdLN directly contributes to systemic persistence.

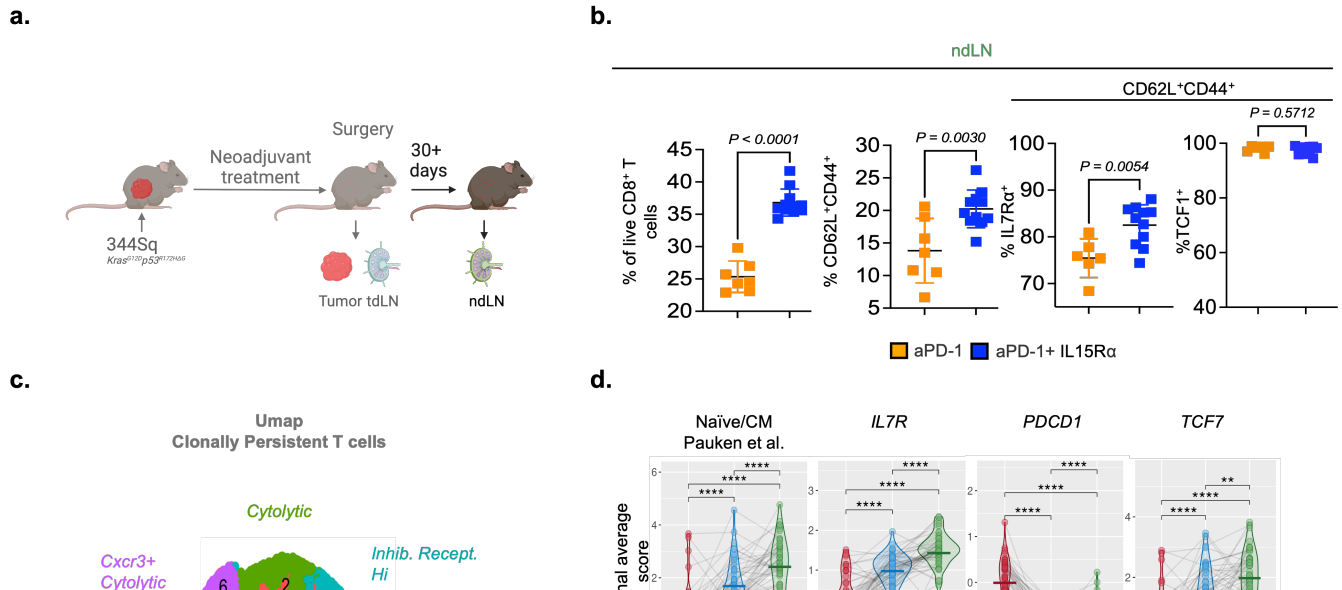

897

898

899

900

901

902

903

904

905

906

907

908

909 **Fig. 5.** $CD8^+$ T cell clonal response in tdLN directly contributes to systemic persistence. **a**. Experimental
910 design, past experimental timepoints until surgery are shown in gray, **b.** Flow cytometry quantification of
911 $CD8^+$ T cells from inguinal non draining lymph node resected more than 30 days after primary tumor
912 resection from mice under neoadjuvant aPD-1 or combination therapy showing percentages of central
913 memory ($CD62L^+CD44^+$) $CD8^+$ T cells expressing IL7Rα and TCF1, **c.** Clustering and UMAP
914 visualization integrating paired CD8T cell clones from tumor, tdLN and ndLN *(n=9321 cells, 52 TM*
915 *clones)* integrated from 9 mice (26 tissues total), colors denote transcriptional clusters, labeled with

functional annotations (top), UMAPs showing cluster location of clones coming from tumor (red), tdLN (blue) and ndLN (green) (bottom), **d.** Violin plots showing clonal average score for Naïve/CM Pauken, Shahid [24], as well as relative expression of IL7R, PDCD1 and TCF7 genes, each line traces and connects matching clones in the tumor (red), tdLN (blue) and non-draining lymph node (ndLN) (green), **e.** Clonal persistence in ndLN more than 30 days post resection of primary tumor (left) from total tumor relevant clones initially identified at moment of surgery per treatment, Z score for IL7R expression in persistent clones (right). Statistics used were *t-test* **(b.), (d.), (e.)**.

Fig. 6. Neoadjuvant Il-15Rα + aPD-1 relies on the tdLN for primary tumor control and induces a robust antitumor protection that is only lost upon simultaneous $CD8^+$ and $CD4^+$ T cell depletion.

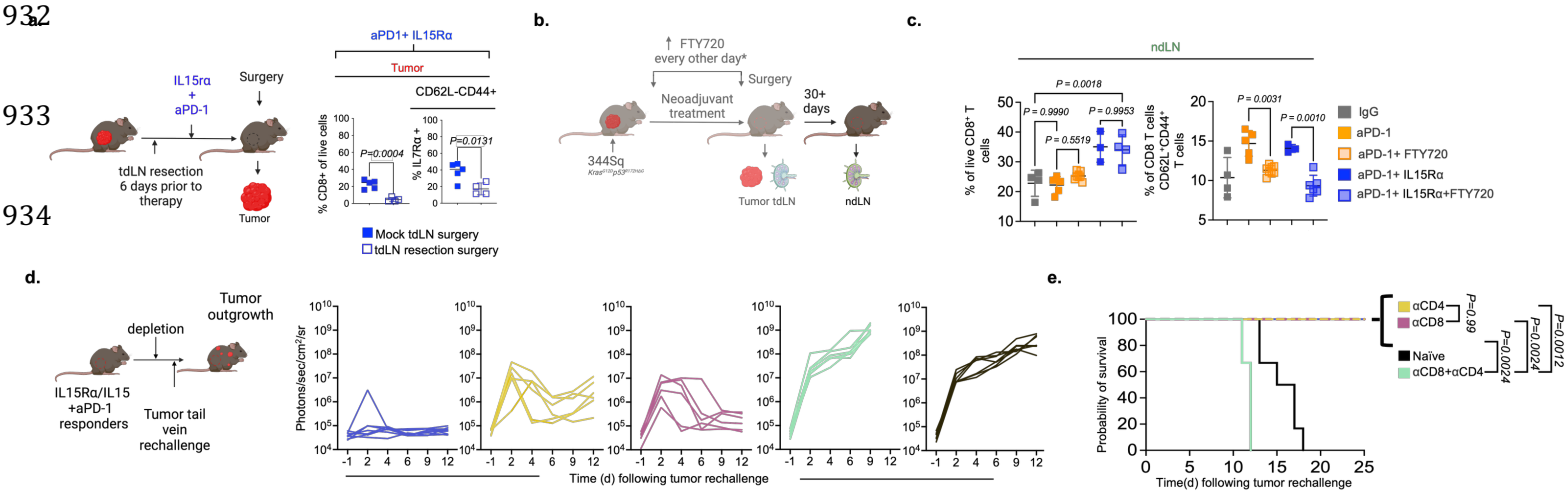

935

936

937

938

939

940

941

942

943

944

945

946

947

948 **Fig. 6.** Neoadjuvant Il-15Rα + aPD-1 relies on the tdLN for primary tumor control and induces a robust
949 antitumor protection that is only lost upon simultaneous $CD8^+$ and $CD4^+$ T cell depletion **a.** Experimental
950 design of tdLN resection experiments (left) and quantification of CD8+ T cells and percentage of IL7R
951 expressing CD8 T cells in the primary tumor **b.** Experimental design for FTY720 experiments, **c.** Flow
952 cytometry quantification of $CD8^+$ T cells from the non-draining lymph node resected 30 days after primary
953 tumor resection from mice receiving neoadjuvant aPD-1 or combination therapy +/- FTY720 showing

954 percentages of CD8$^+$ T cells as well as subsets of central memory T cells, **d.** Schematic design of
955 depletion/tumor rechallenge experiments for combination treated long term responders (left), and BLI
956 plots of tumor burden to the chest after tail-vein injection of combination treated mice with no depletion
957 (blue), or receiving different depleting antibodies:CD4 (yellow), CD8 (purple) CD4/CD8 (green), and
958 naïve age match mice(black), **e.** Overall survival for experimental groups in e. Statistics used were *t-test*
959 **(a.),(c.),** and siddaks log-rank Mantel–Cox test **(e.)**.

960

961

962

963

964

965

966

967

968 **Fig. 7.** CD8$^+$ T cells in tumor draining lymph nodes of NSCLC patients have a distinct clonal response to
969 neoadjuvant aPD-1 treatment.

970

971

972

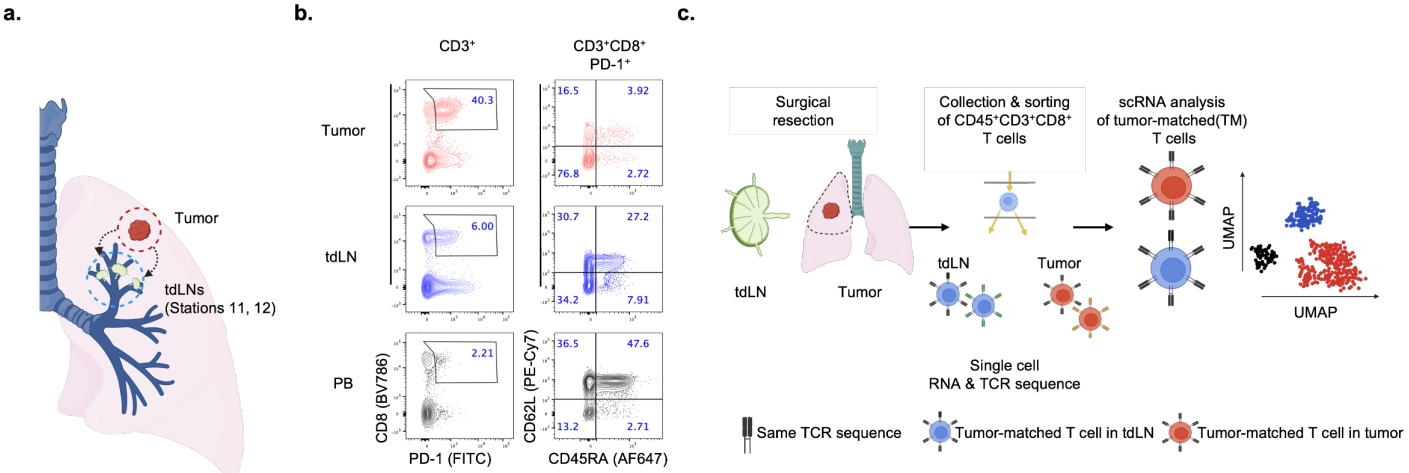

973

974

975

976

977

978

979

980

981

982

983

984

985

986 **Fig. 7.** $CD8^+$ T cells in tumor draining lymph node of NSCLC patients have a distinct clonal response to
987 neoadjuvant aPD-1 treatment. **a.** Schematic representation of tumor and nodal stations, **b.** Representative
988 flow cytometry plots of $CD8^+$ T cells in the tumor, tumor draining lymph node (tdLN) and peripheral
989 blood (PB) showing expression of CD62L,CD45RA and PD-1, **c.** Experimental design for single cell RNA
990 sequence (scRNAseq) experiments, **d.** Schematic representation and relevant clinical features of three
991 patients treated with neoadjuvant aPD-1 therapy with complete response (CR), partial response (PR), no

992 response (NR) and a non-treated patient (NT) selected for single cell sequencing, response is defined by
993 residual viable tumor (RVT) **e.** Clustering and UMAP visualization of tumor matched clones from paired
994 tumor and tdLN integrated from 4 patients (total of 8 samples 14,464 tm expanded T cells). Colors denote
995 transcriptional clusters, labeled with functional annotations (left), UMAP showing tumor (red) and tdLN
996 (blue) clonal distribution (top right), and quiescent Lowery, Krishna [39] and exhausted signature Li, Dan
997 P. Zandberg [50] relative expression (bottom right), **f.** Violin plots showing Z score for T cells for central
998 memory (TCM) Galletti, De Simone [51] & stem central memory (TSCM) Zhang, Zhou [49], Cytotoxic-
999 like and terminal differentiation (Term. diff.) Ciecko, Schauder [47], each line traces and connects
1000 matching clones in the tumor (red) and tdLN (blue), **g.** UMAP showing pseudo-time analysis (left) and Z
1001 score for expression of specific markers: *GZMB, PDCD1, CTLA4, TCF7, SELL, LEF1* as function of
1002 pseudo-time progression (right), **h.** UMAPs showing relative expression of *TCF7, IL7R, TIGIT, GZMB*
1003 (top), and cluster distribution of tumor match clones in clusters defined in **Figure 7.e** per patient in tumor
1004 and tdLN (bottom). Statistics used were paired t-test (f.).

1005

1006

1007

1008 **Extended data fig. 1** Characterization of tumor and tumor draining lymph node CD8^{+} T cells and response
1009 to neoadjuvant aPD-1

1010
1011
1012

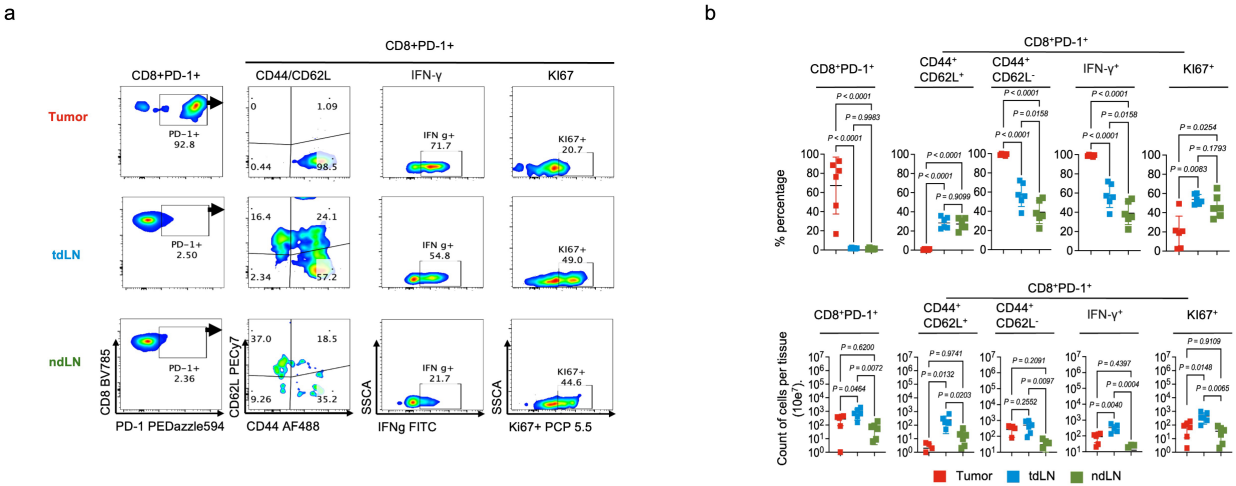

1013

1014

1015

1016

1017

1018

1019

1020

1021

1022

1023

1024

1025

1026 **Extended data Fig. 1** Characterization of tumor and tumor draining lymph node $CD8^+$ T cells and
1027 response to neoadjuvant aPD-1 **a.** Representative flow cytometry plots of $CD8^+$ T cells from tumor, tdLN
1028 and ndLN at time of tumor resection, **b.** quantification of percentages and counts of $CD8^+$ T cells from
1029 flow cytometry data in a. (*n=6 per* group/tissue*),* **c.** Tumor burden fold change of untreated mice (IgG),
1030 responders and non-responders to aPD-1, **d.** Experimental design (top left), and representative flow plots
1031 of effector memory $CD8^+$ effector memory T cells from tdLNs from responder and non-responder mice

showing expression of IL7Rα, KLRG1 (left), CD62L and Ly6C (right), and percentages of $CD8^+$ effector memory T cells from responder (orange) and non-responder mice (black) expressing IL7Rα and Ly6c, **e.** Heatmap showing mean gene expression of CD8+ T cells in tdLN from aPD-1 responder, aPD-1 non responder and untreated (IgG) mouse (total of 3 mice), **f.** quantification of $CD8^+$ T cells in peripheral blood from long term responders to neoadjuvant aPD-1 therapy treated mice after 2 doses of depleting antibody(white) or control(IgG) treatment(orange). Statistics used were One Way ANOVA **(b.),** t-test **(c.)(d.)** and **(f.)**.

Extended data fig. 2 IL15Ra induces an effector memory CD8+ T cells phenotype in the tumor draining lymph node changing their differentiation trajectory and increasing clonal diversity.

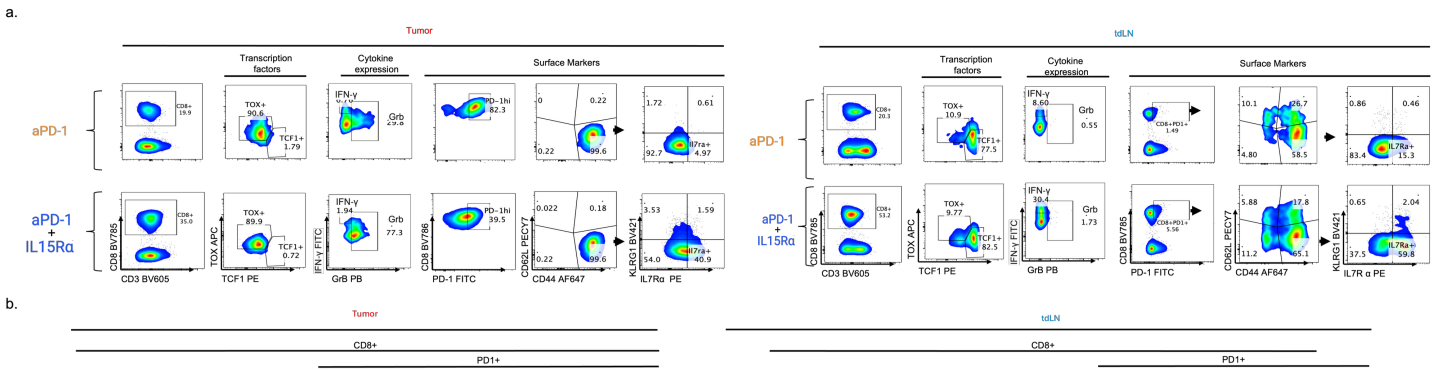

1051

1052

1053

1054

1055

1056

1057

1058

1059

1060

1061

1062

1063

1064 **Extended data Fig. 2** IL15Rα induces an effector memory precursor $CD8^+$ T cells phenotype in the tumor
1065 draining lymph node changing their differentiation trajectory and increasing clonal diversity. **a.**
1066 Representative flow cytometry plots of CD8 T cells from tumor and tdLNs resected at time of survival
1067 surgery from mice treated with aPD-1 or aPD-1+IL-15Rα for the expression of transcription factors
1068 (TCF1,TOX), Cytokine expression (IFN-γ,Grb) and surface markes (PD-1,CD44,C62L,IL7Rα,KLRG1),
1069 **b.**, **c.** Quantification of flow cytometry data by percentage and counts, (*n= 3-5 per group),* **d.**

quantification of central memory populations in the tdLN at time of tumor resection showing expression of IL7Ra, Statistics used were one way ANOVA **(b)**, **(c)**, **(d)**.

Extended data Fig. 3 Single cell sequencing shows differences in CD8^{+}T cell repertoire dynamics induced by treatment **.**

a.

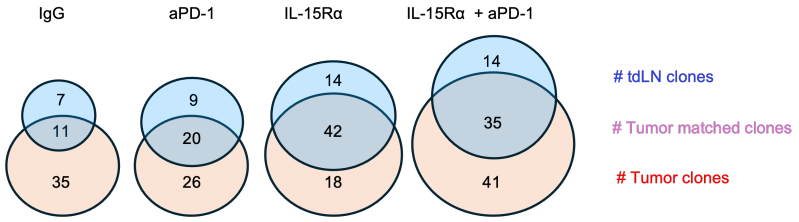

b.

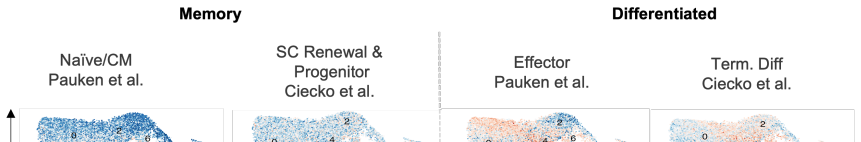

1088

1089

1090

1091

1092

1093

1094

1095

1096

1097

1098

1099

1100

1101 **Extended data Fig. 3** Single cell sequencing shows differences in $CD8^{+}$T cell repertoire dynamics
1102 induced by treatment **a.** Venn diagram showing number of clones from tumor (red) , tdLN (blue) and
1103 overlapping clones between both tissues (tumor matched clones) from different treatments, **b.** UMAP
1104 showing relative expression of memory[24, 47], differentiated[24, 47], cytolytic[24, 49] and
1105 trafficking[48, 52] signatures, **c.** Z score for cytotoxic[49], KILR effector [31], activation & migration[48],

IL7R and Gzmb (Granzyme B) for tumor match clones in the tumor and the tdLN from different treatments. Statistical analysis were t-test **(c.)**.

Extended data Fig. 4 IL15Ra increases the proportion of central memory CD8 T cells that express IL7Ra.

a.

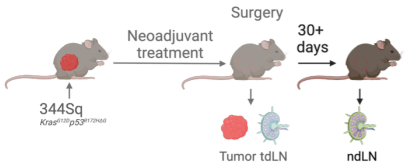

b.

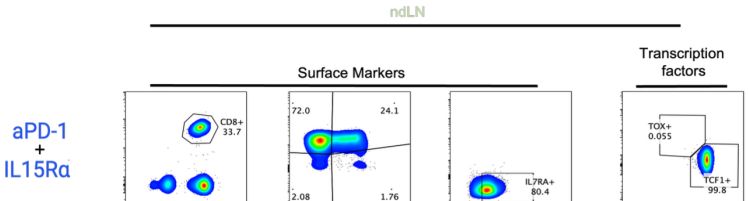

1124

1125

1126

1127

1128

1129

1130

1131

1132

1133

1134

1135

1136

1137 **Extended data Fig. 4** IL-15Rα increases the proportion of central memory $CD8^+$ T cells that express

1138 IL7Rα **a**. Experimental scheme, **b.** Representative flow cytometry plots of CD8+ T cells from tumor and

1139 tdLN of aPD-1 and aPD-1+IL15Rα treated mice showing expression of surface markers

1140 (CD62L,CD44,KLRG1,IL7Ra), and transcription factors (TOX, TCF1), **c.** and **d.** quantification of flow

1141 cytometry data by counts and percentages statistics used were t test **(c)**, **(d).**

Extended data Fig. 5 pseudotime analysis shows differences in CD8^{+}T cell fates.

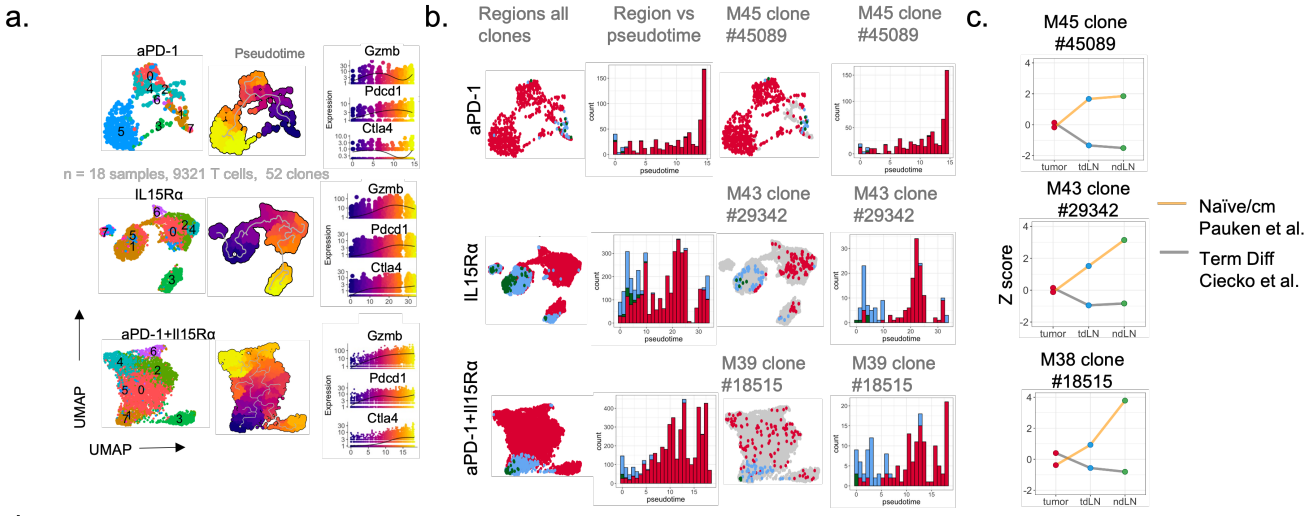

1159

1160

1161

1162

1163

1164

1165

1166

1167

1168

1169

1170

1171

1172 **Extended data Fig. 5** pseudotime analysis shows differences in $CD8^{+}$T cell fates **a.** UMAP showing
1173 pseudotime progression per treatment integrating TM clones from tumor, tdLN and ndLN and Z score
1174 for expression of specific markers as function of pseudo-time progression, **b.** UMAP localization of TM
1175 clones per tissue and treatment and quantification of counts of clones through pseudotime progression
1176 (left), as well as per treatment largest clone UMAP localization and quantification of counts of clone
1177 through pseudotime progression (center), **c**. Z score for Naïve and terminal differentiation signatures for

largest clone per treatment in b., **d.** Clonal expansion by clonal persistence showing persistent and non-persistent clones (top) and Z score of *Pdcd1* and IL7R expression in the tdLN (bottom), **e.** Z score for Memory subcluster KILR effector for persisting clones versus non persisting per treatment and further stratified by tdLN and tumor only T cells (left), Received operative characteristic (ROC) curve for tumor and tdLN derived clones. Statistical analysis were t-test **(d)**, **(e), (g).**

Extended data Fig. 6 Neoadjuvant IL-15Rα agonist relies in the tdLN for primary antitumor response while long term memory depends on CD8$^+$ and CD4$^+$ T cell memory protection.

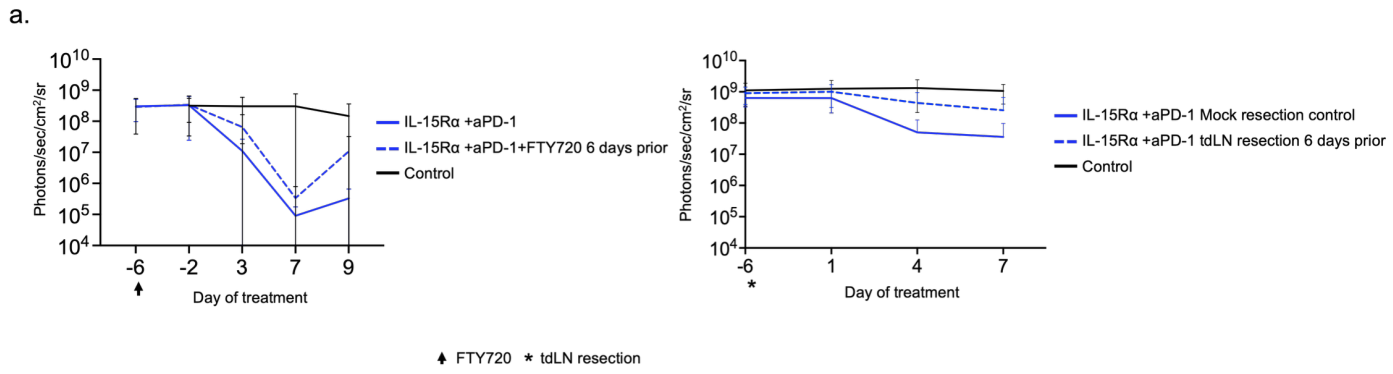

b.

c.

1197

1198

1199

1200

1201

1202

1203

1204

1205

1206

1207

1208

1209

1210 **Extended data Fig. 6** Neoadjuvant IL-15Rα agonist relies in the tdLN for primary antitumor response
1211 while long term memory depends on $CD8^+$ and $CD4^+$ T cell memory protection. **a.** Bioluminescence
1212 imaging plots of combination therapy treated mice that received either FTY720 starting 6 days prior first
1213 dose of therapy (left) or tdLN resection (right), **b.** Experimental design, **c.** quantification of different
1214 immune populations in peripheral blood from mice under treatment with different depletion antibodies for
1215 tumor rechallenge experiments (total of 2 experiments 3-7 mice per group). **d.** Bioluminescence imaging

plots showing tumor burden of combination therapy long term responders during tumor tail-vein rechallenge under depletion of different subsets of immune cells, **e.** Experimental design and BLI plots of tumor burden during tumor rechallenge in long-term responders to aPD-1 receiving CD4 depletion (red) or IgG control (orange).

Extended data Fig. 7 Tumor and tumor draining lymph node transcriptional signatures of patients treated with neoadjuvant aPD-1 therapy

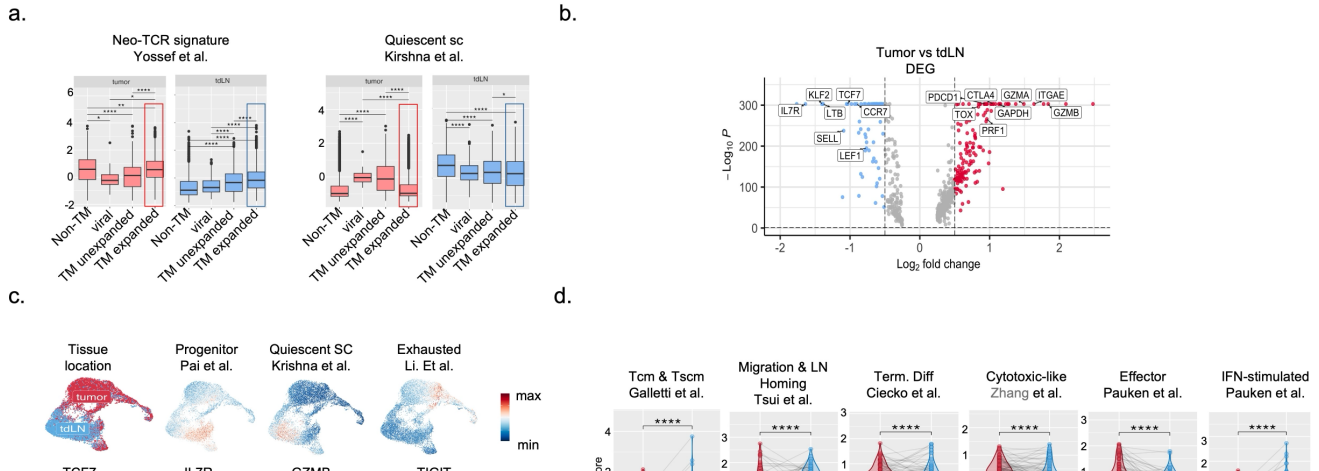

1234

1235

1236

1237

1238

1239

1240

1241

1242

1243

1244

1245

1246

1247

1248 **Extended data Fig. 7** Tumor and tumor draining lymph node transcriptional signatures of patients treated

1249 with neoadjuvant aPD-1 therapy. **a.** Neo-TCR Yossef, Krishna [53] and quiescent (Kirshna et al.)[40]

1250 signature score by tissue sample in Non tumor match (Non-TM), viral, TM unexpanded, TM expanded,

1251 Tumor and tumor draining lymph node transcriptional signatures of patients treated with neoadjuvant

aPD-1 therapy**, b.** plot of differentially expressed genes (DEG) between tumor and tdLN T cells, **c.** UMAP showing overlap of tdLN and tumor T cells as well as expression of progenitor, quiescent, exhausted signatures and genes (top) , and expression of specific genes (bottom), **d.** Average Z score for Tcm & Tscm (Galletti et al.)[51], Migration & LN Homing (Tsui et al.)[52], Term. Diff (Ciecko et al.)[47], Cytotoxic-like (Zhang et al.)[49], Effector (Pauken et al.), IFN-stimulated (Pauken et al.) signatures per clone[24], each line traces and connects matching clones in the tumor (red) and tdLN (blue), **e.** UMAP visualization of tumor match CD8+ T cell clones from neoadjuvant aPD-1 Colors denote transcriptional clusters, labeled with functional annotations from figure 1e (top left), tumor, and tdLN clone localization on UMAP (top middle, left), pseudotime progression though UMAP (top middle, right) and counts of clones through pseudotime progression (top right), UMAP localization of largest clone in memory cluster 2 (C2) (left column), largest clone in progenitor exhausted cluster 1 (C1) (left middle column) and representative small clone (right middle column) from aPD-1 treated patients (NR, PR, CR), clones are color coded for tissue of origin (tumor=red, tdLN=blue), quantification of counts of clones through pseudotime progression are also shown (right column), **f.** Clonal average Z scores for inhibitory receptor, granzyme-like, and IFN-stimulated (Pauken et al.)[24] signatures for patients without treatment (NT) or receiving neoadjuvant aPD-1 with different responses (NR= non-responder, PR=partial responder, CR=complete responder), **g.** Representative flow cytometry plots from tumor and tdLN (level 11) from pathological complete responder (WCM 2050b) at moment of surgery showing CD8+T cell subsets expression of CD62L,CD45RA and IL7Rα markers, **h.** Bar plot showing percentage of persistent $CD8^+$ T cell clones from total expanded clones in blood in complete responder patient at 6 months follow up. Statistics used were t-test **(a.)**,**(f.),**and paired t-test**(d.)**.

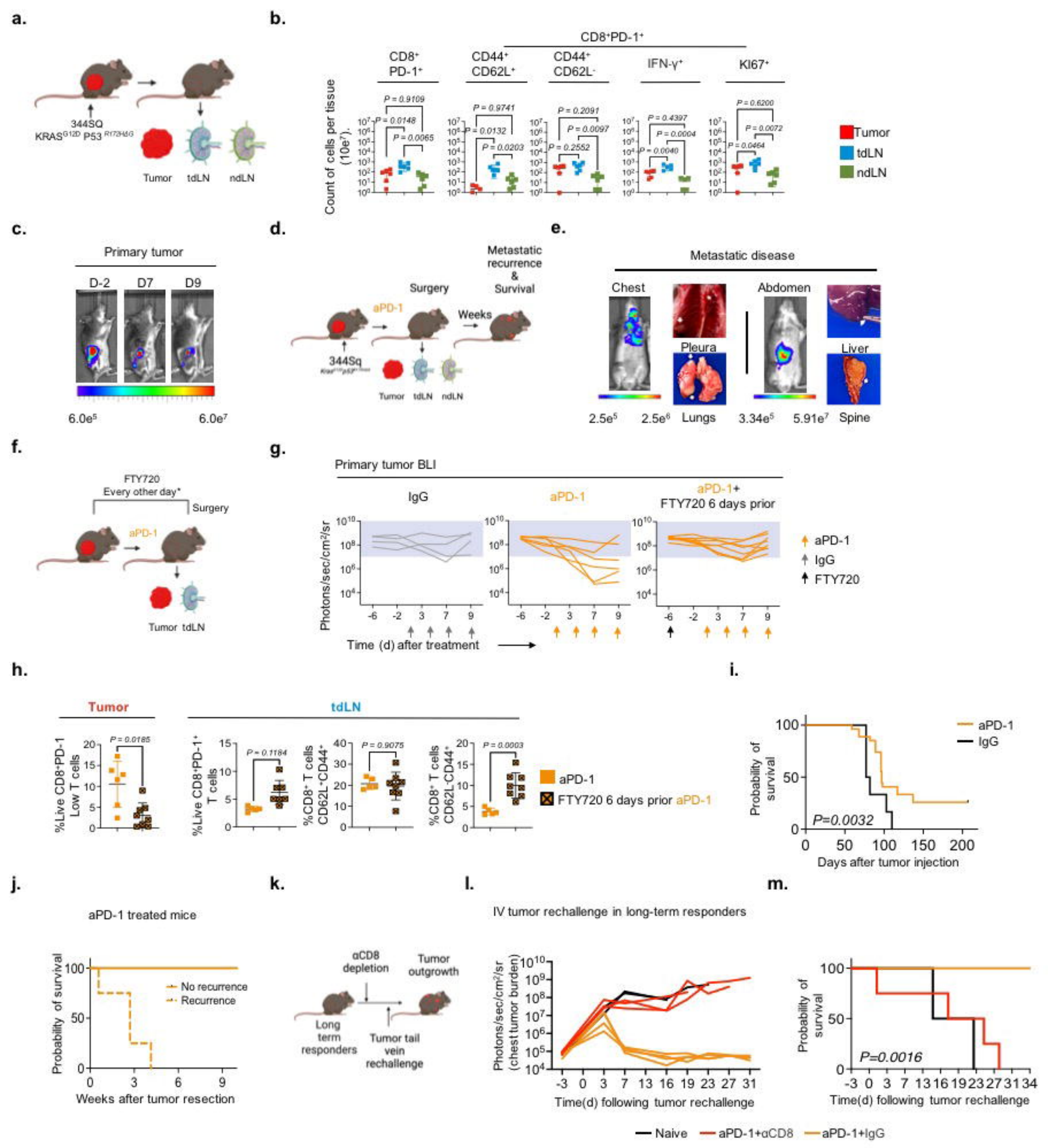
a.
344SQ
KRAS G12D P53 R172H/G
Tumor
tdLN
ndLN
b.
CD8+PD-1+
CD8+ PD-1+
CD44+ CD62L+
CD44+ CD62L-
IFN-γ+
KI67+
Count of cells per tissue (10e7).
P = 0.9109
P = 0.0148
P = 0.0065
P = 0.9741
P = 0.0132
P = 0.0203
P = 0.2091
P = 0.0097
P = 0.2552
P = 0.4397
P = 0.0004
P = 0.0040
P = 0.6200
P = 0.0072
P = 0.0464
Tumor
tdLN
ndLN
c.
Primary tumor
D-2
D7
D9
6.0e5
6.0e7
d.
Metastatic recurrence & Survival
Surgery
aPD-1
Weeks
344Sq
Tumor
tdLN
ndLN
e.
Metastatic disease
Chest
Pleura
Abdomen
Liver
2.5e5
2.5e6
Lungs
3.34e5
5.91e7
Spine
f.
FTY720
Every other day*
Surgery
aPD-1
Tumor
tdLN
g.
Primary tumor BLI
IgG
aPD-1
aPD-1+ FTY720 6 days prior
Photons/sec/cm2/sr
Time (d) after treatment
aPD-1
IgG
FTY720
h.
Tumor
tdLN
%Live CD8+PD-1 Low T cells
P = 0.0185
%Live CD8+PD-1+ T cells
P = 0.1184
%CD8+ T cells CD62L-CD44+
P = 0.9075
%CD8+ T cells CD62L-CD44+
P = 0.0003
aPD-1
FTY720 6 days prior aPD-1
i.
Probability of survival
aPD-1
IgG
P=0.0032
Days after tumor injection
j.
aPD-1 treated mice
Probability of survival
No recurrence
Recurrence
Weeks after tumor resection
k.
αCD8 depletion
Tumor outgrowth
Long term responders
Tumor tail vein rechallenge
l.
IV tumor rechallenge in long-term responders
Photons/sec/cm2/sr (chest tumor burden)
Time(d) following tumor rechallenge
m.
Probability of survival
P=0.0016
Time(d) following tumor rechallenge
Naive
aPD-1+αCD8
aPD-1+IgG

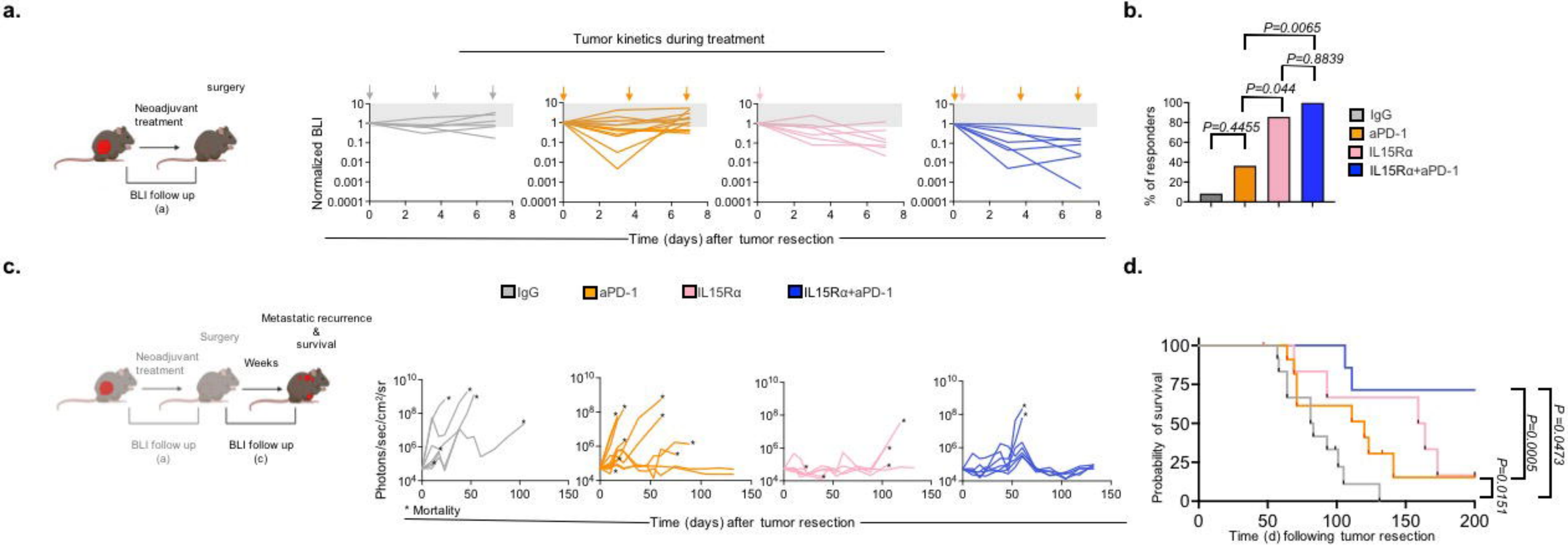
a.
Tumor kinetics during treatment
surgery
Neoadjuvant treatment
BLI follow up (a)
Normalized BLI
Time (days) after tumor resection
b.
P=0.0065
P=0.8839
P=0.044
P=0.4455
% of responders
IgG
aPD-1
IL15Rα
IL15Rα+aPD-1
c.
IgG
aPD-1
IL15Rα
IL15Rα+aPD-1
Metastatic recurrence & survival
Surgery
Neoadjuvant treatment
Weeks
BLI follow up (a)
BLI follow up (c)
Photons/sec/cm²/sr
* Mortality
Time (days) after tumor resection
d.
Probability of survival
Time (d) following tumor resection
P=0.0473
P=0.0005
P=0.0151

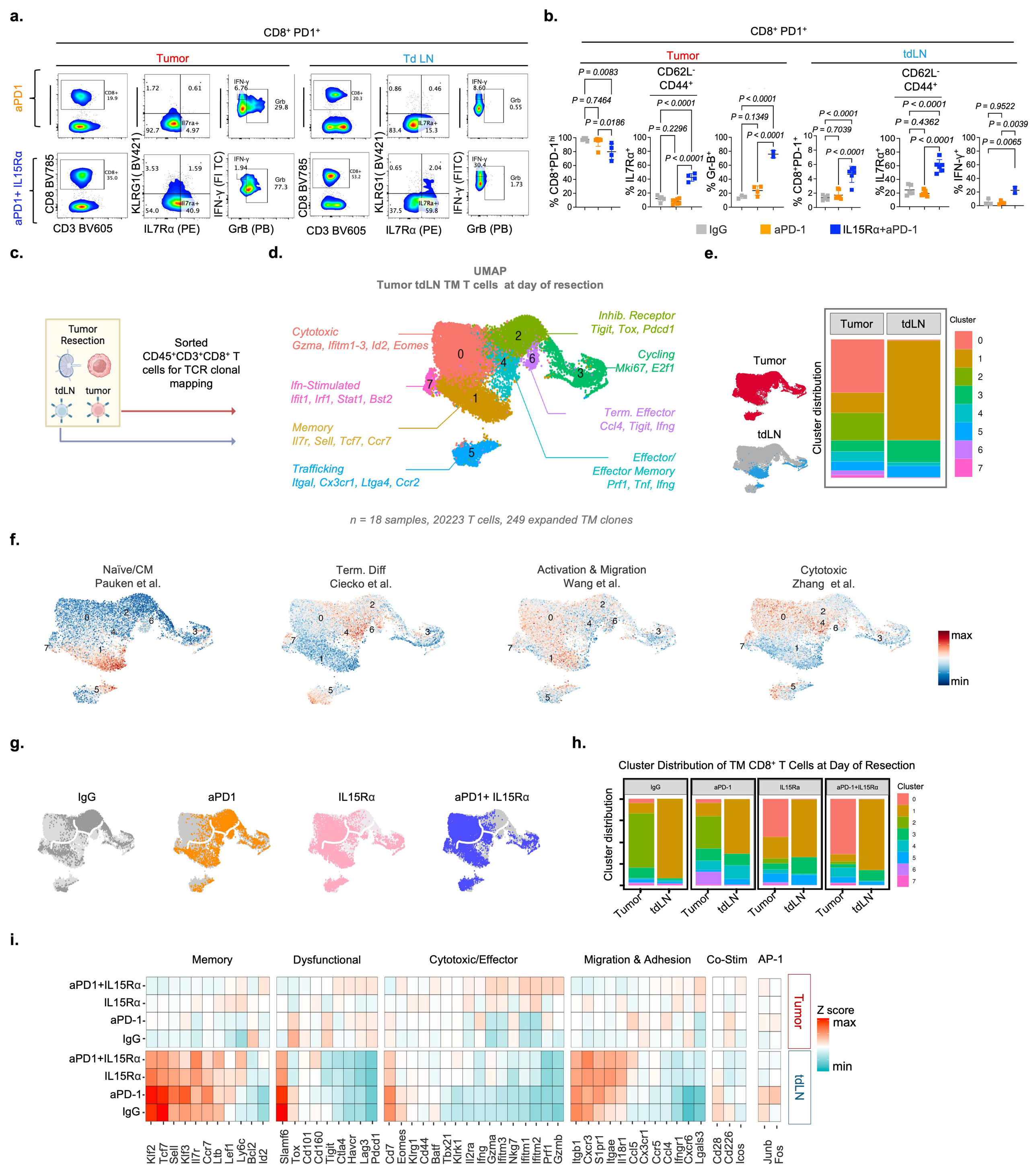
a.
CD8+ PD1+
Tumor
Td LN
aPD1
aPD1+ IL15Rα
CD8 BV785
CD3 BV605
KLRG1 (BV421)
IL7Rα (PE)
IFN-γ (FITC)
GrB (PB)
b.
CD8+ PD1+
Tumor
tdLN
CD62L- CD44+
% CD8+PD-1hi
% IL7Rα+
% Gr-B+
% CD8+PD-1+
% IFN-γ+
IgG
aPD-1
IL15Rα+aPD-1
c.
Tumor Resection
tdLN
tumor
Sorted CD45+CD3+CD8+ T cells for TCR clonal mapping
d.
UMAP
Tumor tdLN TM T cells at day of resection
Cytotoxic
Gzma, Ifitm1-3, Id2, Eomes
Ifn-Stimulated
Ifit1, Irf1, Stat1, Bst2
Memory
Il7r, Sell, Tcf7, Ccr7
Trafficking
Itgal, Cx3cr1, Ltga4, Ccr2
Inhib. Receptor
Tigit, Tox, Pdcd1
Cycling
Mki67, E2f1
Term. Effector
Ccl4, Tigit, Ifng
Effector/
Effector Memory
Prf1, Tnf, Ifng
n = 18 samples, 20223 T cells, 249 expanded TM clones
e.
Tumor
tdLN
Cluster distribution
Cluster
f.
Naïve/CM
Pauken et al.
Term. Diff
Ciecko et al.
Activation & Migration
Wang et al.
Cytotoxic
Zhang et al.
max
min
g.
IgG
aPD1
IL15Rα
aPD1+ IL15Rα
h.
Cluster Distribution of TM CD8+ T Cells at Day of Resection
Cluster distribution
Cluster
i.
Memory
Dysfunctional
Cytotoxic/Effector
Migration & Adhesion
Co-Stim
AP-1
aPD1+IL15Rα
IL15Rα
aPD-1
IgG
Tumor
tdLN
Z score
max
min
Klf2 Tcf7 Sell Klf3 Il7r Ccr7 Ltb Lef1 Ly6c Bcl2 Id2
Slamf6 Tox Cd101 Cd160 Tigit Ctla4 Havcr Lag3 Pdcd1
Cd7 Eomes Klrg1 Cd44 Batf Tbx21 Klrk1 Il2ra Ifng Gzma Ifitm3 Nkg7 Ifitm1 Ifitm2 Prf1 Gzmb
Itgb1 Cxcr3 S1pr1 Itgae Il18r1 Ccl5 Cx3cr1 Ccr5 Ccl4 Ifngr1 Cxcr6 Lgals3
Cd28 Cd226 Icos
Junb Fos

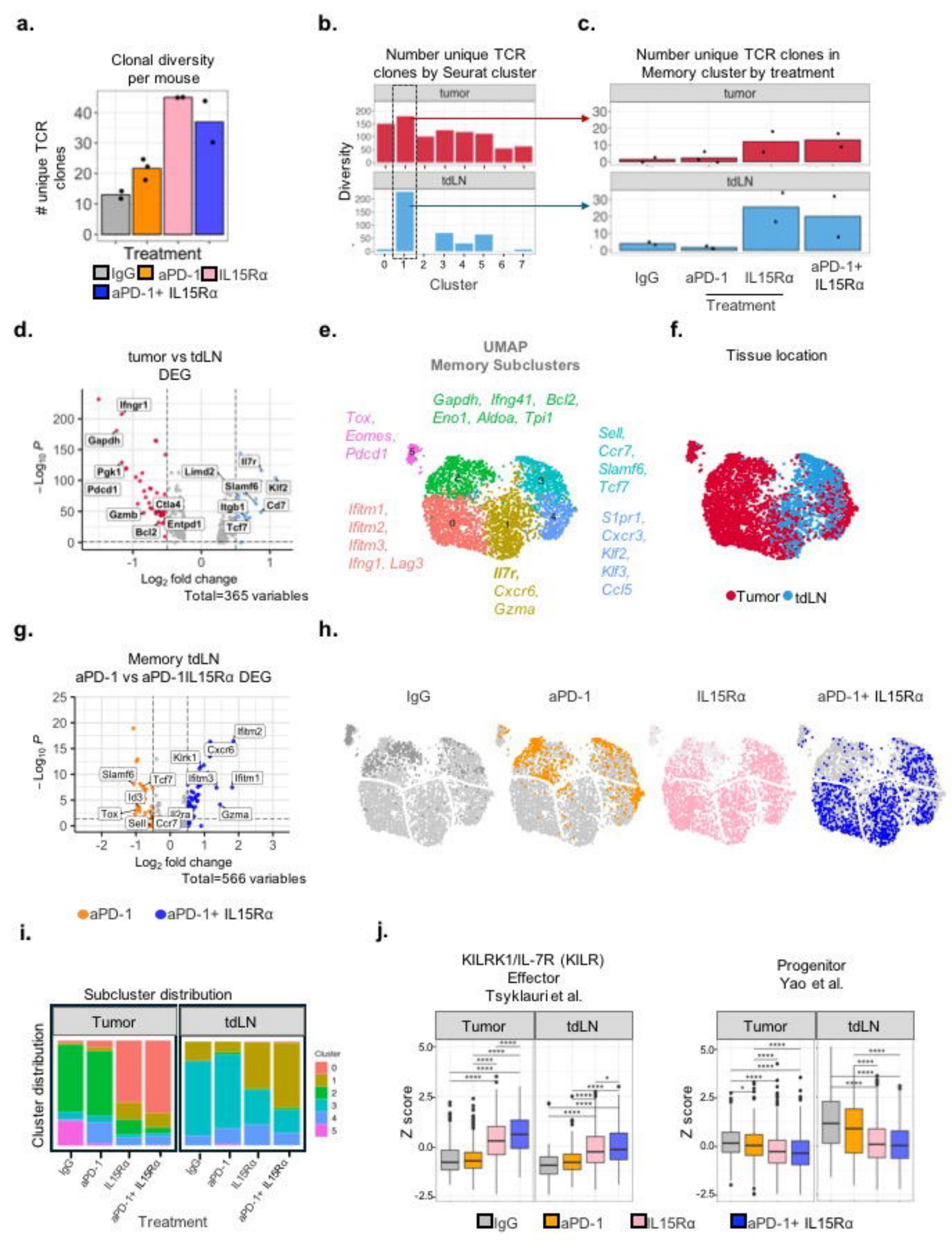
a.
Clonal diversity per mouse
unique TCR clones
Treatment
IgG
aPD-1
IL15Rα
aPD-1+ IL15Rα
b.
Number unique TCR clones by Seurat cluster
tumor
tdLN
Diversity
Cluster
c.
Number unique TCR clones in Memory cluster by treatment
tumor
tdLN
IgG
aPD-1
IL15Rα
aPD-1+ IL15Rα
Treatment
d.
tumor vs tdLN DEG
Ifngr1
Gapdh
Pgk1
Pdcd1
Gzmb
Bcl2
Ctla4
Entpd1
Lmnd2
Slamf6
Il7r
Klf2
Itgb1
Cd7
Tcf7
Log2 fold change
Total=365 variables
e.
UMAP
Memory Subclusters
Gapdh, Ifng41, Bcl2, Eno1, Aldoa, Tpi1
Tox, Eomes, Pdcd1
Sell, Ccr7, Slamf6, Tcf7
Ifitm1, Ifitm2, Ifitm3, Ifng1, Lag3
S1pr1, Cxcr3, Klf2, Klf3, Ccl5
Il7r, Cxcr6, Gzma
f.
Tissue location
Tumor
tdLN
g.
Memory tdLN
aPD-1 vs aPD-1IL15Rα DEG
Ifitm2
Cxcr6
Klrk1
Slamf6
Tcf7
Ifitm3
Ifitm1
Id3
Tox
Il2ra
Gzma
Sell
Ccr7
Log2 fold change
Total=566 variables
aPD-1
aPD-1+ IL15Rα
h.
IgG
aPD-1
IL15Rα
aPD-1+ IL15Rα
i.
Subcluster distribution
Tumor
tdLN
Cluster distribution
Cluster
Treatment
j.
KILRK1/IL-7R (KILR) Effector Tsyklauri et al.
Progenitor Yao et al.
Tumor
tdLN
Z score
IgG
aPD-1
IL15Rα
aPD-1+ IL15Rα

a.

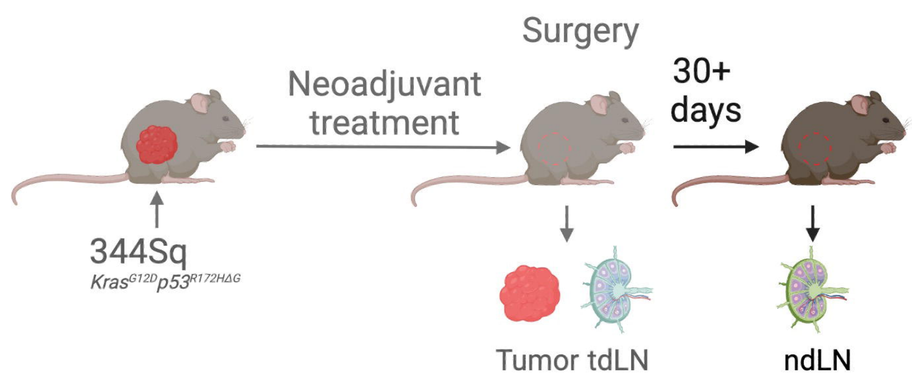
Surgery
Neoadjuvant treatment
30+ days
344Sq
Kras^G12D p53^R172HΔG
Tumor tdLN
ndLN

b.

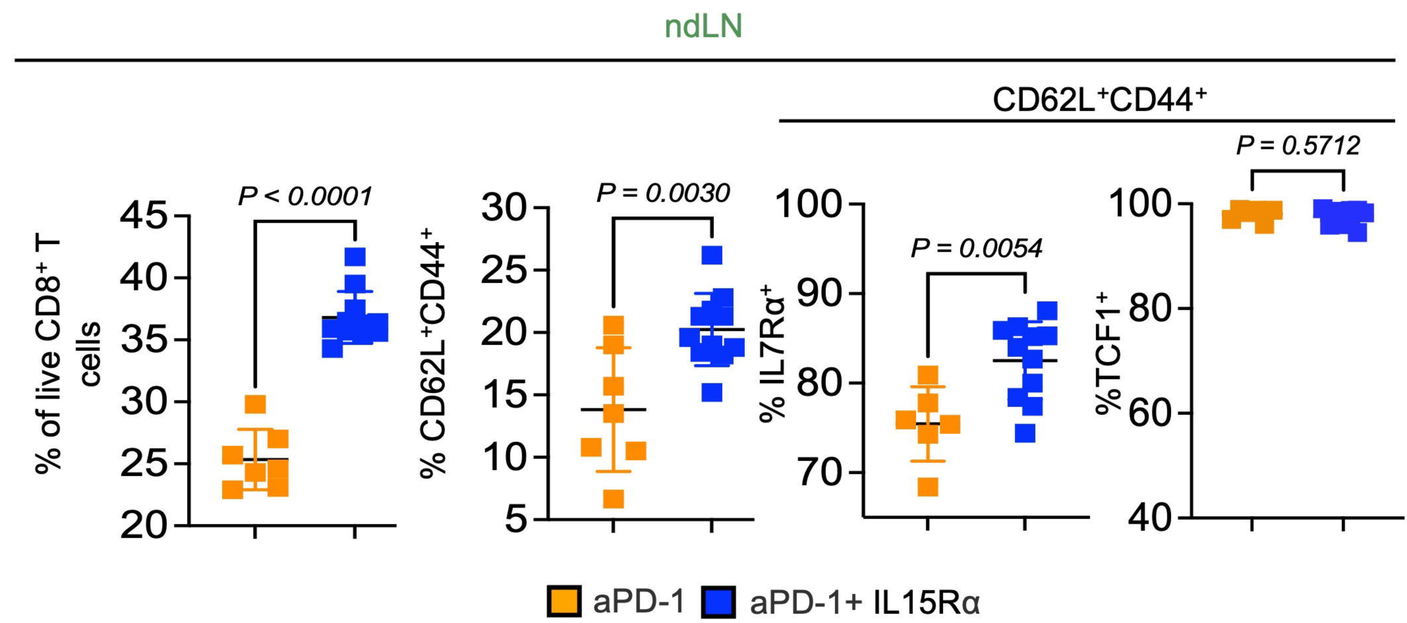
ndLN
CD62L+CD44+
% of live CD8+ T cells
P < 0.0001
% CD62L+CD44+
P = 0.0030
% IL7Rα+
P = 0.0054
%TCF1+
P = 0.5712
aPD-1
aPD-1+ IL15Rα

c.

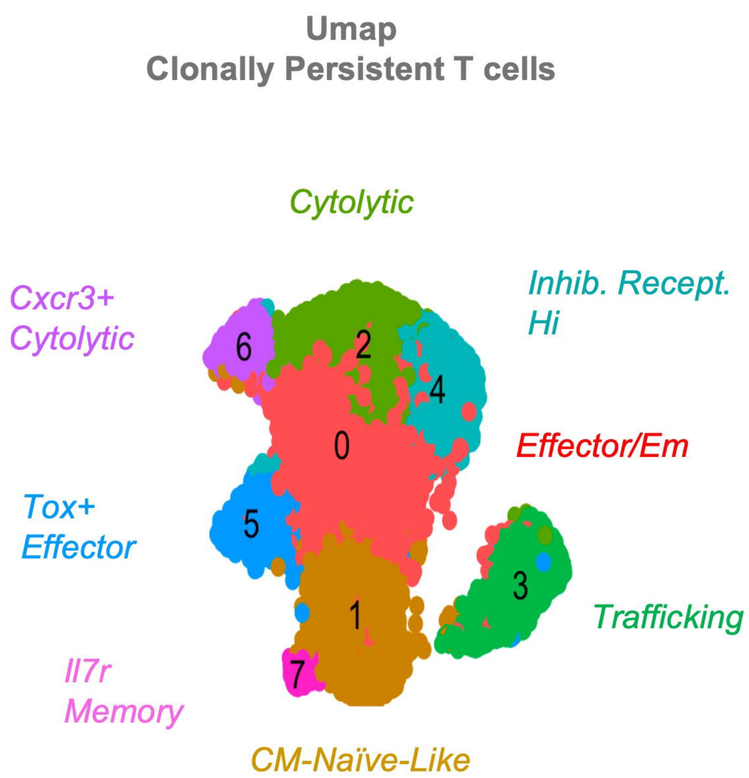
Umap
Clonally Persistent T cells
Cytolytic
Cxcr3+ Cytolytic
Inhib. Recept. Hi
Effector/Em
Tox+ Effector
Trafficking
Il7r Memory
CM-Naïve-Like
n = 26 samples, 9321 t cells, 52 TM clones

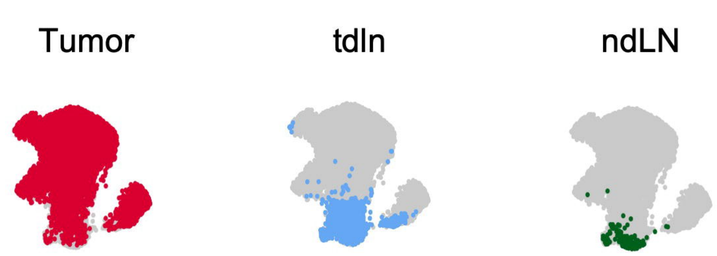
Tumor
tdln
ndLN

d.

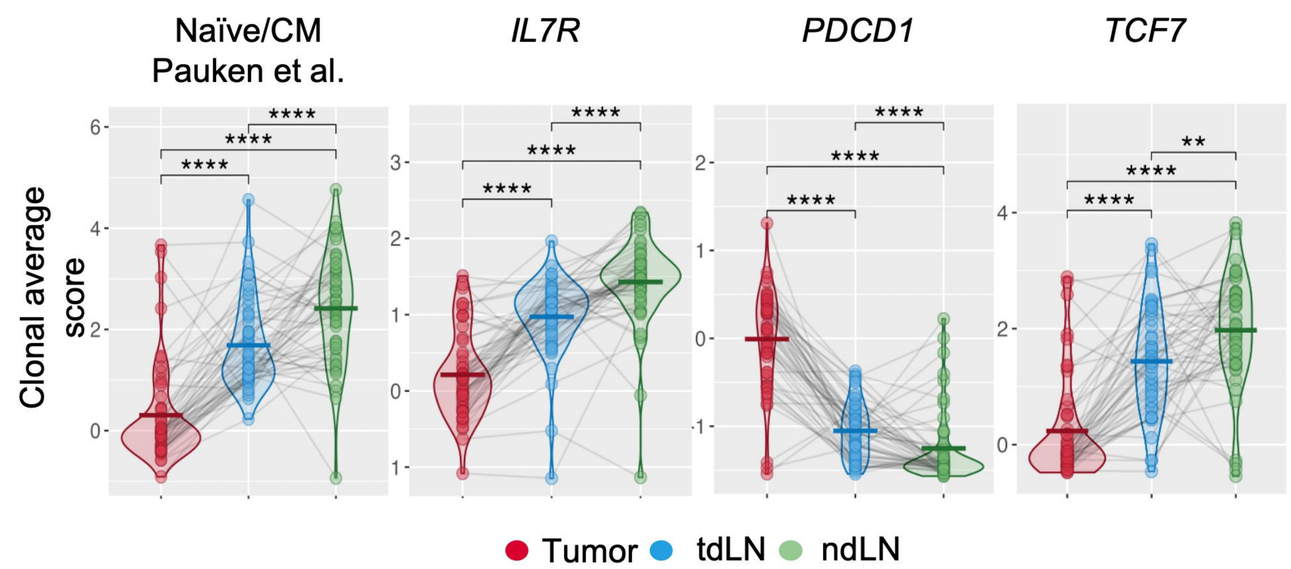
Naïve/CM Pauken et al.
IL7R
PDCD1
TCF7
Clonal average score
Tumor
tdLN
ndLN

e.

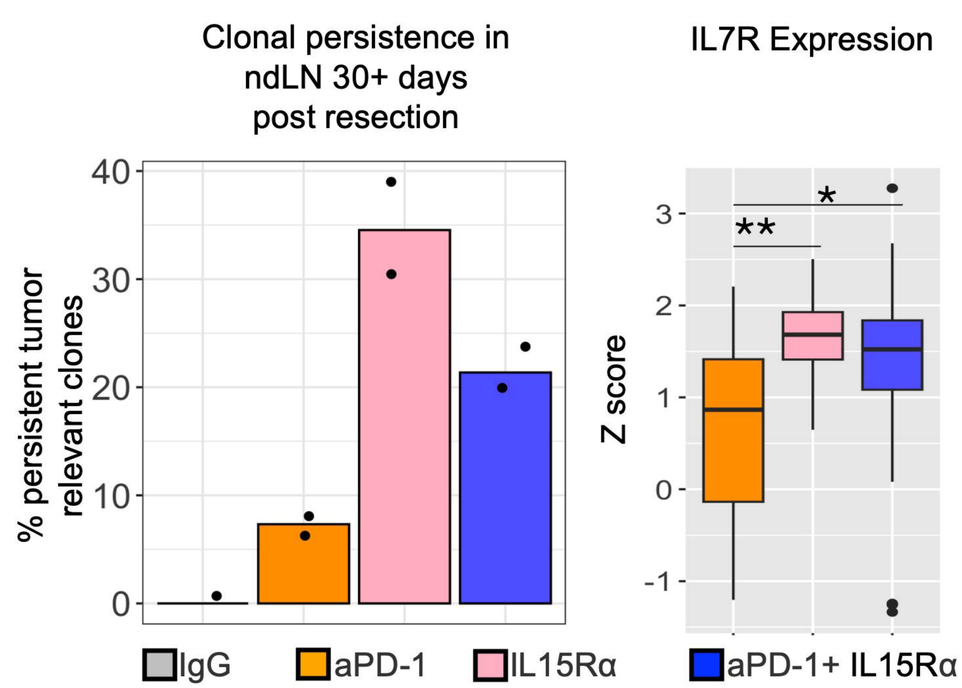
Clonal persistence in ndLN 30+ days post resection
% persistent tumor relevant clones
IL7R Expression
Z score
IgG
aPD-1
IL15Rα
aPD-1+ IL15Rα

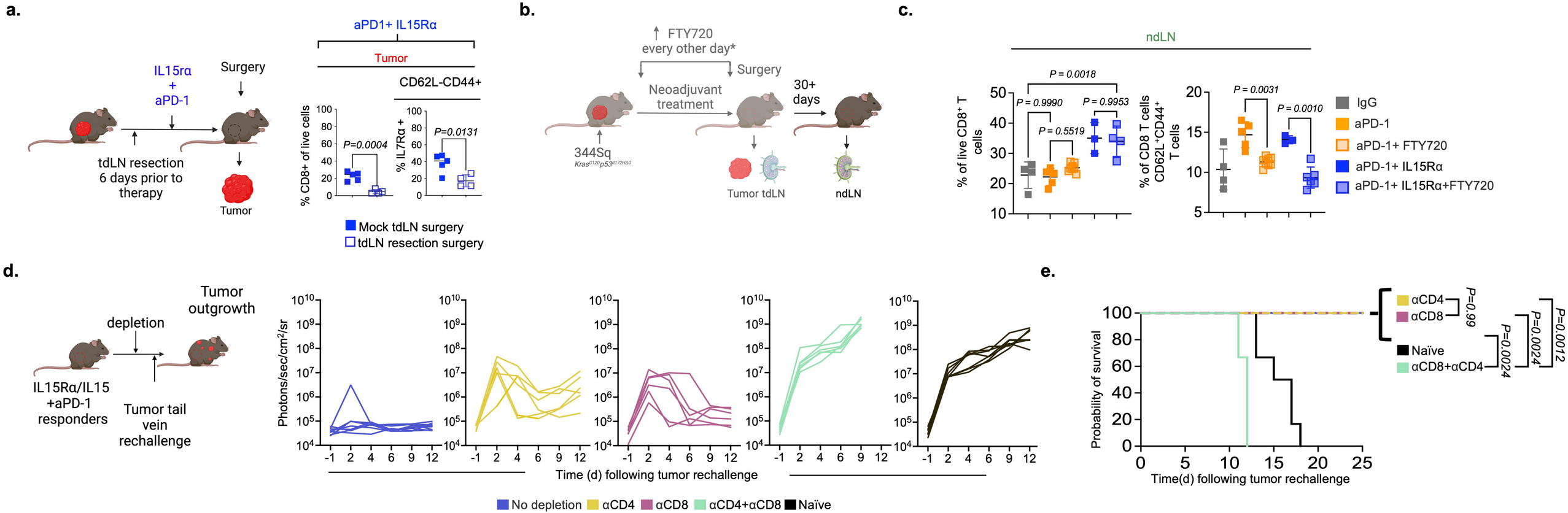
a.
IL15rα
+
aPD-1
Surgery
tdLN resection
6 days prior to
therapy
Tumor
aPD1+ IL15Rα
Tumor
CD62L-CD44+
% CD8+ of live cells
P=0.0004
% IL7Rα +
P=0.0131
Mock tdLN surgery
tdLN resection surgery
b.
FTY720
every other day*
Surgery
Neoadjuvant
treatment
30+
days
344Sq
Tumor tdLN
ndLN
c.
ndLN
% of live CD8+ T cells
P = 0.0018
P = 0.9990
P = 0.9953
P = 0.5519
% of CD8 T cells CD62L+CD44+ T cells
P = 0.0031
P = 0.0010
IgG
aPD-1
aPD-1+ FTY720
aPD-1+ IL15Rα
aPD-1+ IL15Rα+FTY720
d.
depletion
Tumor
outgrowth
IL15Rα/IL15
+aPD-1
responders
Tumor tail
vein
rechallenge
Photons/sec/cm²/sr
Time (d) following tumor rechallenge
No depletion
αCD4
αCD8
αCD4+αCD8
Naïve
e.
Probability of survival
Time(d) following tumor rechallenge
αCD4
αCD8
P=0.99
Naïve
αCD8+αCD4
P=0.0024
P=0.0012

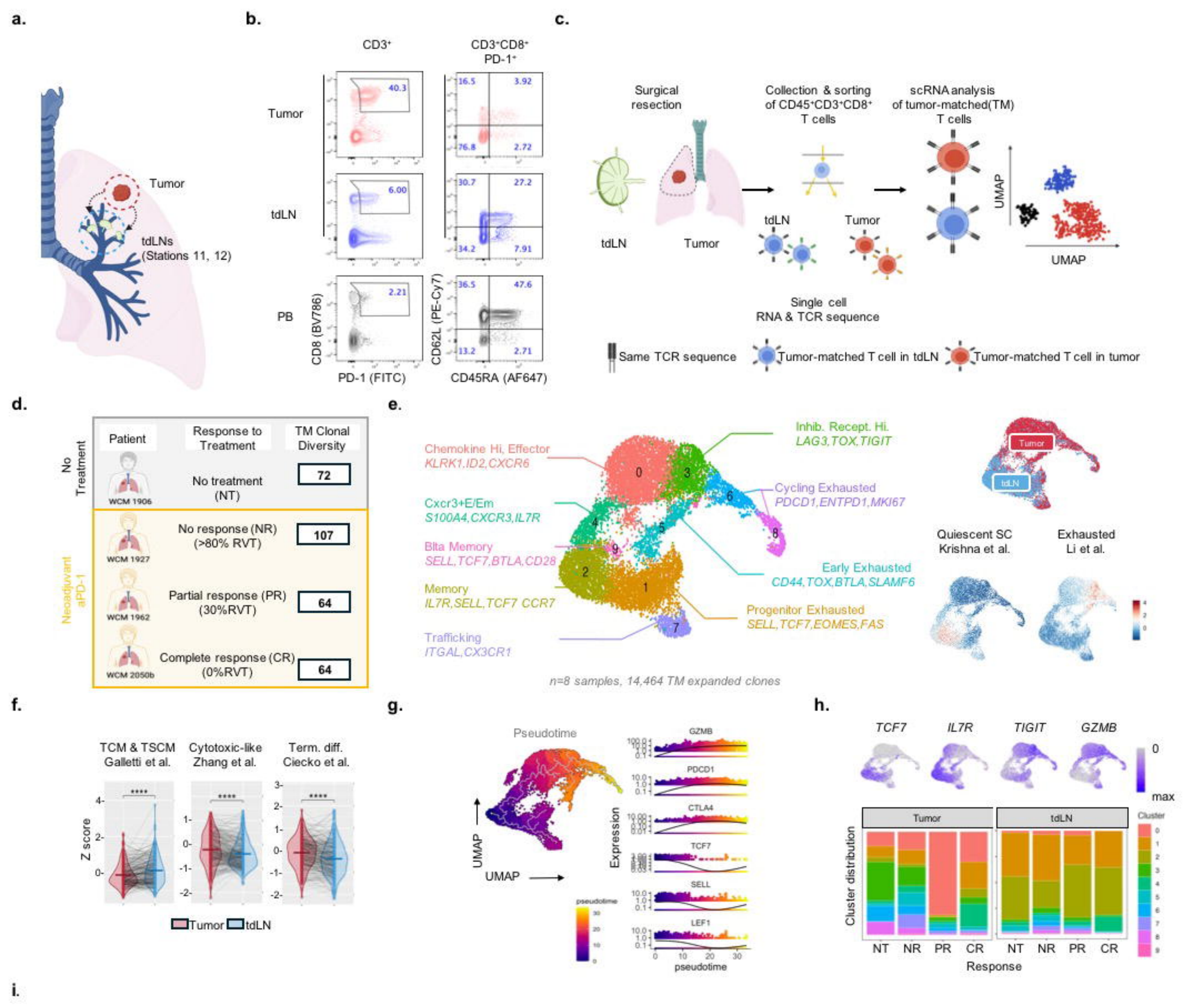
a.
Tumor
tdLNs
(Stations 11, 12)
b.
CD3+
CD3+CD8+
PD-1+
Tumor
tdLN
PB
40.3
6.00
2.21
16.5
3.92
76.8
2.72
30.7
27.2
34.2
7.91
36.5
47.6
13.2
2.71
CD8 (BV786)
PD-1 (FITC)
CD62L (PE-Cy7)
CD45RA (AF647)
c.
Surgical
resection
Collection & sorting
of CD45+CD3+CD8+
T cells
scRNA analysis
of tumor-matched(TM)
T cells
tdLN
Tumor
UMAP
UMAP
Single cell
RNA & TCR sequence
Same TCR sequence
Tumor-matched T cell in tdLN
Tumor-matched T cell in tumor
d.
Patient
Response to
Treatment
TM Clonal
Diversity
No
Treatment
WCM 1906
No treatment
(NT)
72
Neoadjuvant
aPD-1
WCM 1927
No response (NR)
(>80% RVT)
107
WCM 1962
Partial response (PR)
(30%RVT)
64
WCM 2050b
Complete response (CR)
(0%RVT)
64
e.
Chemokine Hi, Effector
KLRK1,ID2,CXCR6
Inhib. Recept. Hi.
LAG3,TOX,TIGIT
Cycling Exhausted
PDCD1,ENTPD1,MKI67
Cxcr3+E/Em
S100A4,CXCR3,IL7R
Blta Memory
SELL,TCF7,BTLA,CD28
Memory
IL7R,SELL,TCF7 CCR7
Trafficking
ITGAL,CX3CR1
Early Exhausted
CD44,TOX,BTLA,SLAMF6
Progenitor Exhausted
SELL,TCF7,EOMES,FAS
0
1
2
3
4
5
6
7
8
9
n=8 samples, 14,464 TM expanded clones
Tumor
tdLN
Quiescent SC
Krishna et al.
Exhausted
Li et al.
f.
TCM & TSCM
Galletti et al.
Cytotoxic-like
Zhang et al.
Term. diff.
Ciecko et al.
Z score
****
Tumor
tdLN
g.
Pseudotime
UMAP
UMAP
Expression
GZMB
PDCD1
CTLA4
TCF7
SELL
LEF1
pseudotime
pseudotime
h.
TCF7
IL7R
TIGIT
GZMB
0
max
Tumor
tdLN
Cluster distribution
Cluster
NT
NR
PR
CR
Response
i.